METHODS

Cell culture and stable expression of TAP–TERT. The human cell lines 293T, MCF7, HeLa, HeLa S3 and VA-13 were maintained in DMEM supplemented with 10% heat-inactivated FBS. BJ fibroblasts were cultured as described[4]. Amphotropic retroviruses were created as described[5,6] using the vectors pWZL-Blast-N-Flag/HA-TERT (for HeLa-S3-TAP–TERT), pBABE-puro or pBABE-puro-TERT. After infection, cells were selected with blasticidin S (10 μg ml^{-1}) for 5 days or with puromycin (2 μg ml^{-1}) for 3 days.

Purification of TERT complexes and cloning of RNAs. HeLa S3 cells (2×10^8) expressing or lacking (control) TAP–TERT were lysed in 5 ml of lysis buffer A (20 mM Tris-HCl, pH 7.4, 150 mM NaCl, 0.5% NP-40, 0.1 mM dithiothreitol (DTT)) and incubated for 30 min on ice. The lysate was then pelleted by centrifugation (16,000*g*) for 20 min at 4 °C. The supernatant was incubated with anti-Flag (M2) antibody-conjugated agarose overnight at 4 °C. The beads were washed three times with lysis buffer A and eluted with 3× Flag peptide (150 ng μl^{-1}). The resulting elution was incubated with Protein A Sepharose beads and an anti-HA antibody (F7; Santa Cruz) for 4 h at 4 °C. The beads were washed three times with lysis buffer A, and RNA was isolated using TRIzol (Invitrogen). RNA samples prepared in this manner were analysed using an Experion capillary electrophoresis device (Bio-Rad) to visualize RNA species. For RNA cloning and the sequencing, the same samples were separated using a 7 M urea/15% polyacrylamide gel, and RNAs recovered from gel were cloned using a small RNA cloning Kit (TaKaRa).

RNA preparation for immunoprecipitation RT–PCR. RNA samples that were prepared from the HeLa S3 cells expressing TAP–TERT as described earlier were also subjected to RT–PCR. For immunoprecipitation of endogenous TERT complexes, cells (1×10^8) were lysed in 600 μl of lysis buffer A, sonicated and pre-cleared with 15 μl of 50% slurry of Protein A Sepharose (Pierce) for 2 h at 4 °C. The pre-cleared total cell lysate was incubated with a rabbit polyclonal anti-TERT antibody (Rockland, 2 μl) for 3 h at 4 °C, followed by incubation with 30 μl of 50% slurry of Protein A Sepharose overnight at 4 °C. After binding, the beads were washed three times for 30 min with lysis buffer A. RNA derived from a single immunoprecipitation was isolated from the Protein A Sepharose using TRIzol (Invitrogen) followed by RT–PCR with primers specific for *TERC*, *RMRP* or *RNase P*. Although other RNAs also co-purified with human TERT (Supplementary Table 1), we failed to confirm the interaction of *Alu* sequences or the 5.8S ribosomal RNA on the Y chromosome with TERT (data not shown).

RT–PCR and quantitative RT–PCR. Either total cellular RNA or RNA from immunoprecipitation was isolated using TRIzol (Invitrogen) and subjected to RT–PCR. The following primers were used: *TERC* (43F, 5′-TCTAACCC TAACTGAGAAGGGCGT-3′ and 163R, 5′-TGCTCTAGAATGAACGGTGGA AGG-3′), *RMRP* (F5, 5′-TGCTGAAGGCCTGTATCCT-3′ and R257, 5′-TGAGAATGAGCCCCGTGT-3′), *RNase P* (F50, 5′-GTCACTCCACTCC CATGTCC-3′ and R318, 5′-AATTGGGTTATGAGGTCCC-3′), and the human β-actin gene (also known as *ACTB*) (5′-CAAGAGATGGCCACGGCTGCT-3′ and 5′-TCCTTCTGCATCCTGTCGGCA-3′). The reverse transcription reaction was performed for 60 min at 42 °C using the recovered RNA, and PCR was immediately performed (22 cycles for 293T cells, and 26 cycles for HeLa cells: 94 °C, 30 s; 60 °C, 30 s; 72 °C, 30 s).

Quantitative RT–PCR (qRT–PCR) was performed with a LightCycler 480 II (Roche) according to the manufacturer's protocols. The expression levels of *RMRP* were detected using the following primers and probe; forward primer, 5′-GAGAGTGCCACGTGCATACG-3′, reverse primer, 5′-CTCAGCGGGATA-CGCTTCTT-3′, VIC-labelled TaqMan MGB probe, 5′-ACGTAGACATT-CCCC-3′. β-actin was used as a reference.

Total *RMRP* was detected using primers (F5, 5′-TGCTGAAGGCC TGTATCCT-3′ and R257, 5′-TGAGAATGAGCCCCGTGT-3′) that amplify both endogenous and ectopically introduced *RMRP*. In Fig. 4a, for VA-13, BJ and MCF7 cells, reverse transcription was performed using random hexamers (GE Healthcare) and ectopically expressed *RMRP* was detected with vector-specific primers (F5, 5′-TGCTGAAGGCCTGTATCCT-3′ and LKO.1-RT, 5′-ACTGCCATTTGTCTCGAGGT-3′). For HeLa cells, reverse transcription was performed with pQC3′ (5′-AAGCGGCTTCGGCCAGTAACGTTA-3′) and PCR was performed with the primers F5 (5′-TGCTGAAGGCCTGTATCCT-3′) and R257 (5′-TGAGAATGAGCCCCGTGT-3′). Northern blotting and qRT–PCR experiments (Supplementary Fig. 14) confirmed that the differences in *RMRP* levels that were observed using the RT–PCR conditions used in Fig. 4a accurately reflect *RMRP* levels. Signal intensity was measured with ImageJ software.

Telomerase activity reconstituted *in vitro* and TRAP assay. *In vitro* reconstitution of telomerase activity (telomere-specific reverse transcriptase activity) was performed as described previously[5]. In brief, recombinant TERT was expressed in the TnT T7-Coupled Reticulocyte Lysate System (Promega) following the manufacturer's instructions. Purified *TERC* or *RMRP* was included in the *in vitro* transcription/translation reactions. The telomeric repeat amplification protocol (TRAP)[7–9] was used to detect telomere-specific reverse transcriptase activity.

Affinity purification of recombinant GST–TERT fusion proteins. GST–TERT–HA, GST–TERT-HT1 and GST–TERT-DN in the pGENKZ expression vector[10] were provided by S. Murakami. Bacteria (BL21-Gold) containing these vectors were plated at 30 °C overnight and then a single colony was picked to inoculate liquid cultures, which were incubated at 37 °C overnight. Thereafter 1 ml of this culture was re-inoculated into 100 ml of Luria-Bertani medium, incubated at 37 °C for 4 h without isopropyl-β-D-thiogalactoside (IPTG) induction, collected by centrifugation, suspended in a lysis buffer (20 mM Tris-HCl, pH 7.4, 150 mM NaCl, 0.5% NP-40, 0.1 mM DTT, 10 mM phenylmethyl sulphonyl fluoride (PMSF), proteinase inhibitor (Nacalai Tesque)) and sonicated twice for 10 s at 4 °C. After centrifugation of the sonicated lysates, the supernatants were passed through DEAE-Sepharose, and the GST-fusion proteins were recovered using glutathione-Sepharose 4B beads. The resin was washed with lysis buffer A at least three times, and the GST-fusion proteins were then eluted with glutathione at 4 °C for 1 h (20 mM glutathione (reduced form)) in elution buffer (50 mM Tris-HCl, pH 8.8, 150 mM NaCl, 0.5% NP-40, 0.1 mM DTT, 10 mM PMSF, proteinase inhibitor (Nacalai Tesque)). Supplementary Fig. 6 shows that wild type and TERT-DN were produced at similar levels using this method and the effects of incubation time and IPTG on yield. The average yield for this method is 500 ng (5 ng μl^{-1}) of active form of TERT from 100 ml culture.

RdRP assay. The affinity purified recombinant GST–TERT fusion protein (10 ng) was incubated with 1 μg of full length *RMRP* RNA or truncated *RMRP* products (*RMRP* 1–200, *RMRP* 1–120 and *RMRP* 1–60 for Fig. 2i) transcribed *in vitro* (SP6) in 200 mM KCl, 50 mM Tris-HCl, pH 8.3, 10 mM DTT, 30 mM $MgCl_2$, 50 μM rATP, 50 μM rGTP, 50 μM rCTP and 2 μCi of [α-^{32}P]UTP at 32 °C for 2 h. To perform the experiments under low salt conditions, 20 μl of 0.2× SSC was then added to adjust final salt concentration to 15 mM NaCl and 1.5 mM sodium citrate, whereas 20 μl of 4× SSC was added to adjust final salt concentration to 300 mM NaCl and 30 mM sodium citrate to achieve high salt conditions. These mixtures were incubated at 37 °C for a further 1 h. Resulting products were treated with proteinase K to stop the reaction and purified with phenol–chloroform. To ensure that RNA products were completely denatured, we performed both conventional formamide treatment (with 95% formamide/20 mM EDTA gel-loading buffer at 95 °C for 5 min) and a further treatment with 1 M de-ionized glyoxal at 65 °C for 15 min.

To analyse double-stranded RNA produced by the TERT–*RMRP* complex, we performed this RdRP assay and treated the products with bacterial RNase III (*E. coli*, Ambion; 50 mM NaCl, 10 mM Tris-HCl, pH 7.9, 1 mM DTT, 10 mM $MgCl_2$) or RNase T1 (Roche; 50 mM Tris-HCl, pH 8.3, 300 mM NaCl and 30 mM sodium citrate).

Northern blotting. Total RNA and small RNAs (<200 nucleotides in length) were isolated using a mirVana miRNA Isolation Kit (Ambion) according to the manufacturer's protocol. Total RNA or small RNA (10 μg) was separated on denaturing polyacrylamide gels, then blotted onto Hybond-N+ membranes (GE Healthcare) using a Trans-Blot SD Semi-Dry Transfer Cell (Bio-Rad). Hybridization was performed in Church buffer (0.5 M $NaHPO_4$, pH 7.2, 1 mM EDTA and 7% SDS) containing 10^6 c.p.m. ml^{-1} of each ^{32}P-labelled probe for 14 h. The membranes were washed in 2× SSC, and the signals were detected by autoradiography.

Identification of short RNA species derived from *RMRP*. Using ten consecutive probes corresponding to the *RMRP* sequence, we found that the small RNAs derived from *RMRP* shown in Figs 4e–g and 5a were detected by probes containing the complementary sequences to nucleotides 21–40 of *RMRP*. To determine the function of these *RMRP*-derived small RNAs, we purchased a chemically synthesized siRNA targeting this 20-nucleotide portion of the *RMRP* sequence (siRNA: 5′-GGCTACACACTGAGGACTC-3′; Dharmacon) and transfected this siRNA into HeLa, 293T and MCF7 cells plated on six-well dishes using Lipofectamine 2000 (Invitrogen) according to the manufacturer's protocol.

RNase protection assay. *RMRP* RNA was transcribed with SP6 RNA polymerase in the presence of [α-^{32}P]UTP using RiboMAX Large Scale RNA Production System (Promega). Total cellular RNA (30 μg) was hybridized overnight at 60 °C with equal amounts of ^{32}P-labelled *RMRP* sense probe. Hybrids were digested with RNase A and RNase T1. The protected fragments were separated by PAGE under denaturing conditions and visualized by autoradiography.

Analysis of the chemical structure of the ends of small RNAs. To determine the phosphorylation status of the termini of small RNAs, 30 μg of small RNA (<200 nucleotides in length) was treated with calf intestinal alkaline phosphatase (CIP; TaKaRa) for 2 h at 37 °C. CIP was inactivated by phenol–chloroform extraction. Part of the CIP-treated RNA was then treated with T4 polynucleotide

kinase (TaKaRa) supplemented with 1 mM ATP for 2 h at 37 °C, and phenol–chloroform extraction was performed. Small RNA (15 μg) was treated with T4 polynucleotide kinase without ATP for 2 h at 37 °C. The reaction was inactivated by phenol–chloroform extraction. After overnight sodium acetate–ethanol precipitation at −20 °C, the treated RNAs were resolved by 20% denaturing polyacrylamide/urea gel electrophoresis and then analysed by northern blotting[12,13].

To further analyse the 3′ end of these small RNAs, we performed oxidation and β-elimination reactions. Specifically, the $NaIO_4$ reaction was performed by adding 20 μg of small RNA in water to 5× borate buffer (148 mM borax and 148 mM boric acid, pH 8.6) and freshly dissolved 200 mM $NaIO_4$ to create a final concentration of 1× borate buffer and 25 mM $NaIO_4$. The mixtures were incubated for 10 min at 20 °C. Glycerol was added to quench remaining $NaIO_4$, and the samples were incubated for a further 10 min at 20 °C. For β-elimination, small RNAs were dried by centrifugation and evaporation and dissolved in 50 μl of 1× borax buffer (30 mM borax, 30 mM boric acid and 50 mM NaOH, pH 9.5) and incubated at 45 °C for 90 min. Nucleic acids were recovered by sodium acetate–ethanol precipitation at −20 °C overnight, and the treated RNAs were resolved by 20% denaturing 7 M urea PAGE and analysed by northern blotting[13].

Stable expression of shRNA. We used the pLKO.1-puro vector and the sequences described below to create shRNA vectors specific for *TERT*, *Dicer* and GFP. These vectors were used to make amphotropic retroviruses and polyclonal cell populations were purified with selection with puromycin (2 μg ml^{-1}). The sequences used for the indicated short hairpin RNAs are shown below where the capitalized letters represent the targeting sequences: *TERT* shRNA1, 5′-GGAAGACAGTGGTGAACTTCCctcgagGGAAGTTCACCACTGTCTTCCttttt-3′ and 5′-aattcaaaaaGGAAGACAGTGGTGAACTTCCctcgagGGAAGTTCACCACTGTCTTCC-3′; *TERT* shRNA2, 5′-GGAACACCAAGAAGTTCATCTctcgagAGATGAACTTCTTGGTGTTCCttttt-3′ and 5′-aattcaaaaaGGAACACCAAGAAGTTCATCTctcgagAGATGAACTTCTTGGTGTTCC-3′. *Dicer* sequences: *Dicer* shRNA1, 5′-GCTCGAAATCTTACGCAAATActcgagTATTTGCGTAAGATTTCGAGCttttg-3′ and 5′-aattcaaaaaGCTCGAAATCTTACGCAAATActcgagTATTTGCGTAAGATTTCGAGC-3′; *Dicer* shRNA2, 5′-CCACACATCTTCAAGACTTAActcgagTTAAGTCTTGAAGATGTGTGGttttg-3′ and 5′-aattcaaaaaCCACACATCTTCAAGACTTAActcgagTTAAGTCTTGAAGATGTGTGG-3′.

Immunoprecipitation of human AGO2 complexes. HeLa or 293T cells were lysed in lysis buffer A and immunoprecipitation was performed using pre-immune sera or anti-AGO2 antibodies[48] (provided by H. Siomi and M. C. Siomi). RNA was isolated using TRIzol from the protein A beads and resolved by electrophoresis on 7 M urea 20% PAGE. Small RNAs were detected by northern blotting with an antisense probe, a sense probe derived from nucleotides 21–40 of *RMRP*, or a *miR-16*-specific probe (5′-CGCCAATATTTACGTGCTGCTA-3′).

45. Hahn, W. C. *et al.* Creation of human tumour cells with defined genetic elements. *Nature* 400, 464–468 (1999).
46. Hahn, W. C. *et al.* Inhibition of telomerase limits the growth of human cancer cells. *Nature Med.* 5, 1164–1170 (1999).
47. Kim, N. W. *et al.* Specific association of human telomerase activity with immortal cells and cancer. *Science* 266, 2011–2015 (1994).
48. Yamashita, T. *et al.* RNA-dependent RNA polymerase activity of the soluble recombinant hepatitis C virus NS5B protein truncated at the C-terminal region. *J. Biol. Chem.* 273, 15479–15486 (1998).
49. Azuma-Mukai, A. *et al.* Characterization of endogenous human Argonautes and their miRNA partners in RNA silencing. *Proc. Natl Acad. Sci. USA* 105, 7964–7969 (2008).

MOLECULAR AND CELLULAR BIOLOGY, Apr. 2010, p. 1620–1633 Vol. 30, No. 7
0270-7306/10/$12.00 doi:10.1128/MCB.00810-09

Requirement of ATM for Rapid p53 Phosphorylation at Ser46 without Ser/Thr-Gln Sequences[▽]

Masami Kodama,[1] Chihiro Otsubo,[1,2] Toru Hirota,[3] Jun Yokota,[2] Masato Enari,[1,2]* and Yoichi Taya[1,4]*

Radiobiology Division, National Cancer Center Research Institute,[1] and Biology Division, National Cancer Center Research Institute,[2] 5-1-1 Tsukiji, Chuo-ku, Tokyo 104-0045, Japan; Cancer Institute, Japanese Foundation for Cancer Research, Koto-ku, Tokyo 135-8550, Japan[3]; and Cancer Science Institute of Singapore, National University of Singapore, Center for Life Sciences, #02-07, 28 Medical Drive, Singapore 117456, Singapore[4]

Received 22 June 2009/Returned for modification 8 August 2009/Accepted 15 January 2010

p53 phosphorylation at Ser46 following DNA damage is important for preferential transactivation of proapoptotic genes. Here, we report that ataxia-telangiectasia mutated (ATM) kinase is responsible for Ser46 phosphorylation of p53 during early-phase response to DNA damage. To elucidate the direct phosphorylation of p53 at Ser46 by ATM, an ATM mutant (ATM-AS) sensitive to ATP analogues was engineered. *In vitro* kinase assays revealed that p53 was phosphorylated at Ser46 by ATM-AS, even when ATP analogues were used as phosphate donors, although this phosphorylation site is not in an SQ motif, a consensus ATM site. Furthermore, Ser46 phosphorylation by ATM was dependent on the N- and C-terminal domains of p53, unlike Ser15 phosphorylation. Immunofluorescence analyses showed that Ser46-phosphorylated p53 was observed as foci in response to DNA damage and colocalized with γ-H2AX or Ser1981-phosphorylated ATM. These results suggest that ATM phosphorylates a noncanonical serine residue on p53 by mechanisms different from those for the phosphorylation of Ser15.

The tumor suppressor protein p53 activates the transcription of numerous target genes involved in cell cycle arrest, apoptosis, and DNA repair (5, 15, 35). Upon various cellular stresses, p53 is phosphorylated and acetylated at multiple sites to activate downstream target genes (13, 31, 36).

Phosphorylation of p53 at Ser15 leads to the dissociation of MDM2, an E3 ubiquitin ligase, from p53 to prevent MDM2-dependent p53 degradation (36). We have previously shown that Ser46 on p53 is phosphorylated following DNA damage and that this phosphorylation contributes to the expression of p53-regulated apoptosis-inducing protein 1 (p53AIP1) (33). Ser46 phosphorylation also contributes to the preferential transactivation of other proapoptotic genes, such as Noxa and PUMA, to prevent tumor formation (18, 27). Although p38 mitogen-activated protein (MAP) kinase, protein kinase C δ (PKCδ), homeodomain-interacting protein kinase 2 (HIPK2), and dual-specificity tyrosine phosphorylation-regulated kinase 2 (DYRK2) have been reported to phosphorylate p53 at Ser46 in response to UV or adriamycin (ADR), a radiomimetic DNA-damaging agent, these enzymes are controversial candidates for direct kinases for Ser46 phosphorylation occurring in early phase (within 1 h) in response to ionizing radiation (IR) (6, 11, 16, 41, 49).

Ataxia-telangiectasia mutated (ATM) is a member of the phosphatidylinositol 3-phosphate kinase (PI3-K) family and is crucial for the initiation of signaling pathways following exposure to IR. Functional defects of the gene encoding ATM cause the human genetic disorder ataxia-telangiectasia (A-T). The major hallmarks of A-T are neurodegeneration, immunodeficiency, genomic instability, and cancer predisposition (26). Following exposure to IR, ATM phosphorylates Ser/Thr-Gln (S/T-Q) sequences on numerous proteins participating in DNA damage responses (29). Among these proteins, p53 phosphorylation at Ser15 is a well-known target of ATM (3, 7, 21).

Here, we found that ATM directly phosphorylates p53 at Ser46 as well as Ser15 and that ATM is required for acute DNA damage response to induce Ser46 phosphorylation. Unlike Ser15 phosphorylation, the Ser46 phosphorylation by ATM requires both proline-rich and C-terminal domains of p53. Furthermore, Ser46-phosphorylated p53 is partially colocalized with IR-activated ATM that is known to localize at DNA double-strand break (DSB) sites. Interestingly, Ser46 phosphorylation by IR-activated ATM is induced within 1 h and ATM is required for early-phase response to DNA damage.

MATERIALS AND METHODS

RNA interference (RNAi) experiments and RT-PCR. For the expression of short hairpin RNA (shRNA), oligonucleotides containing sequences homologous to ATM (5′-GATCCCCAAGCTATCAGAGAAGCTAATAAATTCAAGAGATTTATTAGCTTCTCTGATAGCTTTTTTTGGAAA-3′ and 5′-AGCTTTTCCAAAAAAAGCTATCAGAGAAGCTAATAAATCTCTTGAATTTATTAGCTTCTCTGATAGCTTGGG-3′) or to HIPK2 (5′-GATCCCCGAAAGTACATTTTCAACTGTTCAAGAGACAGTTGAAAATGTACTTTCTTTTTGGAAA-3′ and 5′-AGCTTTTCCAAAAAGAAAGTACATTTTCAACTGTCTCTTGAACAGTTGAAAATGTACTTTCGGG-3′) (10) were synthesized and the duplex oligonucleotide DNA was inserted into the pSUPER.retro vector (Oligoengine) to generate pSR-ATM and pSR-HIPK2, respectively. These plasmids

* Corresponding author. Mailing address for Masato Enari: Biology Division, National Cancer Center Research Institute, 5-1-1 Tsukiji, Chuo-ku, Tokyo 104-0045, Japan. Phone: 81-3-3542-2511. Fax: 81-3-3542-0807. E-mail: menari@ncc.go.jp. Mailing address for Yoichi Taya: Cancer Science Institute of Singapore, Center for Life Sciences #02-07, 28 Medical Drive, National University of Singapore, Singapore 117456, Singapore. Phone: 65-6516-8706. Fax: 65-6873-9664. E-mail: csiyt@nus.edu.sg.

▽ Published ahead of print on 1 February 2010.

were digested to obtain DNA fragments containing the H1 promoter and DNA coding for shRNA, and these DNA fragments were inserted into pLenti6.2 V5-DEST (Invitrogen) to generate pL-shATM and pL-shHIPK2, respectively. Lentiviruses were produced in accordance with the manufacturer's instructions (Invitrogen) and used to infect MCF7 or U2OS cells. To generate stable cell lines, infected cells were selected with blasticidin (Invitrogen). The sequences of primers for reverse transcription-PCR (RT-PCR) were as follows: 5′-GGCCTCAC ATGTGCAAGTTTTC-3′ and 5′-TTGGTAGGTATCAAGGAGGCTC-3′ for HIPK2 and 5′-TCCACAGTCTTCTGGGTGGCAGTGA-3′ and 5′-GGGGAG CCAAAAGGGTCATCATCTC-3′ for glyceraldehyde-3-phosphate dehydrogenase (GAPDH). For experiments with short interfering RNA (siRNA), Allstars negative-control siRNA and Hs_ATM_5_HP validated siRNA were purchased from Qiagen. Sequences of siRNAs and primers for RT-PCR for HIPK2 and DYRK2 are described by Hofmann et al. and Taira et al., respectively (17, 41). For p53 knockdown, siRNA described previously was used (12). Each 100 pmol of siRNA was transfected with HiPerfect transfection reagent (Qiagen) and RNAiMax transfection reagent (Invitrogen) into MCF7 or U2OS cells (2×10^5 cells). At 48 h after transfection, cells were used for assays.

Immunoblotting analysis. To prepare whole-cell lysates, cells were collected and stored at −80°C. The cells were thawed in chilled IP150 buffer (50 mM HEPES [pH 7.0], 150 mM NaCl, 1 mM EDTA, 2.5 mM EGTA, 10% glycerol, 1 mM dithiothreitol [DTT], 1 mM Na_3VO_4, and 5 mM NaF) containing 0.1% NP-40 and a protease inhibitor cocktail consisting of 10 μg/ml pepstatin A, 10 μg/ml antipain, 10 μg/ml chymostatin, 10 μg/ml leupeptin, 10 μg/ml E-64, and 10 μg/ml phenylmethylsulfonyl fluoride (PMSF). The lysates were centrifuged for 15 min in a microcentrifuge at 4°C, and the supernatants were collected and boiled in sodium dodecyl sulfate (SDS) sample buffer. The samples were separated on SDS-PAGE gels and blotted onto Immobilon-P transfer membrane (Millipore). The membranes were blocked with blocking solution containing 5% nonfat dry milk in phosphate-buffered saline (PBS) containing 0.1% Tween 20 (PBS-T) for 1 h at room temperature and then incubated with primary antibodies diluted in Can Get Signal Solution 1 (Toyobo) overnight at 4°C. After three washes with PBS-T, the membranes were incubated for 1 h with secondary antibodies in PBS-T containing 1% nonfat dry milk at room temperature. Immunoblots were visualized by chemiluminescence (Western Lightning; Perkin-Elmer). Anti-ATM antibody (2C1) was purchased from GeneTex, Inc.; anti-p53 antibody (9282), anti-phospho-Ser15-of-p53 antibody (9284), and anti-phospho-Thr68-of-Chk2 antibody (2661) were from Cell Signaling Technology; anti-phospho-Ser1981-of-ATM antibody (10H11.E12) was from Rockland Inc.; anti-glutathione *S*-transferase (anti-GST) antibody (B14) was from Santa Cruz Biotechnology; and anti-FLAG (M2) antibody was from Sigma. Antibodies to phospho-Ser392 of p53 were described previously (28, 33, 40). Anti-phospho-Ser46-of-p53 mouse monoclonal antibody was generated with a synthetic phosphorylated peptide (Lab of Monoclonal Antibody Co., Inc.). Signals from immunoblots were quantified by Multi-gauge v.3.0 (Fujifilm).

Plasmids and purification of recombinant proteins. An expression construct of FLAG-tagged wild-type ATM was a gift from M. Kastan. To construct expression vectors for the mutant ATM, parts of the FLAG-tagged wild-type ATM were mutated using a QuikChange site-directed mutagenesis kit (Stratagene). Cells transiently transfected with constructs were thawed in IP150 buffer supplemented with 0.3% Nonidet P-40, followed by centrifugation. ATM was purified using anti-FLAG M2 agarose (Sigma) and then eluted into IP150 buffer with 3× FLAG peptides (Sigma) after two washes with IP150 buffer with 0.3% Nonidet P-40, two washes with IP500 buffer containing 500 mM NaCl with 0.3% Nonidet P-40, and two washes with IP150 buffer without detergent. For kinase assays using ATM-AS, a series of ATMs, including ATM-WT and ATM-KD, were prepared in IP150 or IP500 supplemented with 0.03% Nonidet P-40. GST fusion proteins were expressed in *Escherichia coli* BL21 cells from pGEX-4T-1 or pGEX-6P-1 vectors (GE Healthcare).

In vitro **kinase assay.** ATP was purchased from Cell Signaling Technology, and all ATP analogues were from Biolog. *In vitro* kinase assays were performed in kinase buffer (9802) (25 mM Tris-HCl [pH 7.5], 5 mM β-glycerophosphate, 2 mM dithiothreitol, 0.1 mM Na_3VO_4, and 10 mM $MgCl_2$) (Cell Signaling Technology) supplemented with 10 mM $MnCl_2$ and 0.1 mM ATP or ATP analogues, at 30°C for 30 or 60 min. Reactions were stopped by the addition of SDS sample buffer followed by boiling. Reaction products were subjected to immunoblotting.

Confocal immunofluorescent microscopy. Cells were fixed with 3.7% formaldehyde in PBS for 10 min at room temperature, permeabilized with 0.5% Triton X-100 in PBS for 10 min at room temperature, and then blocked with PBS containing 3% bovine serum albumin (BSA) and 0.1% goat serum for 1 h at room temperature. Cells were incubated with primary antibodies overnight at 4°C and then with secondary antibodies (Alexa Fluor 488 goat anti-rabbit IgG or Alexa Fluor 594 goat anti-mouse IgG; Invitrogen) for 1 h at room temperature. Vectashield with DAPI (4′,6-diamidino-2-phenylindole; Vector Laboratories Inc.) was used as the mounting medium. The primary antibodies used for immunostaining were anti-p53 (Ab-6; Calbiochem), anti-phospho-Ser1981 of ATM (10H11.E12; Rockland Inc.), anti-phospho-Ser15 of p53 (40), anti-phospho-Ser46 of p53 (33), anti-phospho-Thr68 of Chk2 (2661; Cell Signaling Technology), anti-phospho-Ser957 of SMC1 (NB100-205; Novus Biologicals), anti-γ-H2AX (JBW103; Upstate Biotechnology Inc.), and anti-PML antibody (PG-M3; Santa Cruz Biotechnology). All primary antibodies were diluted in Can Get Signal A (Toyobo). These immunostained objects were observed under a confocal immunofluorescent microscope using a Zeiss LSM5 Exciter system equipped with Zen software (Carl Zeiss Inc.). For preextraction experiments, cells were extracted with 0.2% Triton X-100 for 3 min at room temperature prior to 3.7% formaldehyde fixation, followed by the same procedures described above. Fluorescence resonance energy transfer (FRET) signals were obtained as described previously (23). In brief, cells were exposed to 488-nm light to excite Alexa Fluor 488 (donor fluorescence) and the emission of Alexa Fluor 568 (acceptor molecules) was scanned to detect FRET.

RESULTS

ATM is required for p53 phosphorylation at Ser46 following exposure to IR but not to UV. It was reported that Ser46 phosphorylation of p53 is abrogated following exposure to IR in A-T lymphoblasts (38). To identify the kinase that phosphorylates p53 at Ser46 in response to IR, we first assessed whether ATM is required for this phosphorylation in other cell lines. Human mammary carcinoma MCF7 cells were infected with lentiviruses encoding a short hairpin RNA (shRNA) against ATM to generate stable cell lines devoid of ATM expression (pL-shATM) (Fig. 1A). The phosphorylation at Ser46 as well as Ser15 (3, 7, 21) was delayed and attenuated in ATM-depleted cells (Fig. 1B). Similar results were obtained using human osteosarcoma U2OS cells depleted of ATM (Fig. 1C and D). On the other hand, downregulation of ATM expression had no effect on phosphorylation at Ser392 of p53 in either MCF7 or U2OS cells (Fig. 1B and D). In contrast, depletion of ATM had little effect on phosphorylation at Ser46 or Ser15 after exposure to UV (Fig. 1E and F). We also performed immunoblotting to assess Ser46 phosphorylation at various doses of IR. Ser46 phosphorylation was obviously detected at a high dose of IR compared to Ser15 phosphorylation, consistent with previous reports (33) (Fig. 2). These findings suggest that ATM is responsible for the phosphorylation of p53 at Ser46 after exposure to IR but not to UV.

ATM phosphorylates p53 at Ser46 ***in vitro*****.** To examine whether ATM associates with kinases that phosphorylate p53 at Ser46, FLAG-tagged ATM transiently expressed in 293T cells was purified by immunoprecipitation with anti-FLAG antibody and used for *in vitro* kinase assays using full-length p53 fused to GST (GST-p53) as a substrate (Fig. 3A). When wild-type ATM (ATM-WT) was mixed with GST-p53, ATM-WT phosphorylated p53 at Ser46 as well as at Ser15, although neither a kinase-dead ATM mutant (ATM-KD) nor eluates from cells transfected with an empty vector (control) produced the same phosphorylation patterns (Fig. 3A). On the other hand, p53 phosphorylation at Ser392 by ATM was not detected, as shown in Fig. 3A. Given that ATM purified from 293T cells contains the kinase activity to phosphorylate p53 at Ser46, similar experiments were carried out using different cell lines, including human lung carcinoma H1299 and MCF7 cells. Recombinant ATM purified from these cells also phosphorylated p53 at Ser46 as well as Ser15 (Fig. 3B and C), suggesting that the Ser46 kinase activity in the immunoprecipitates was

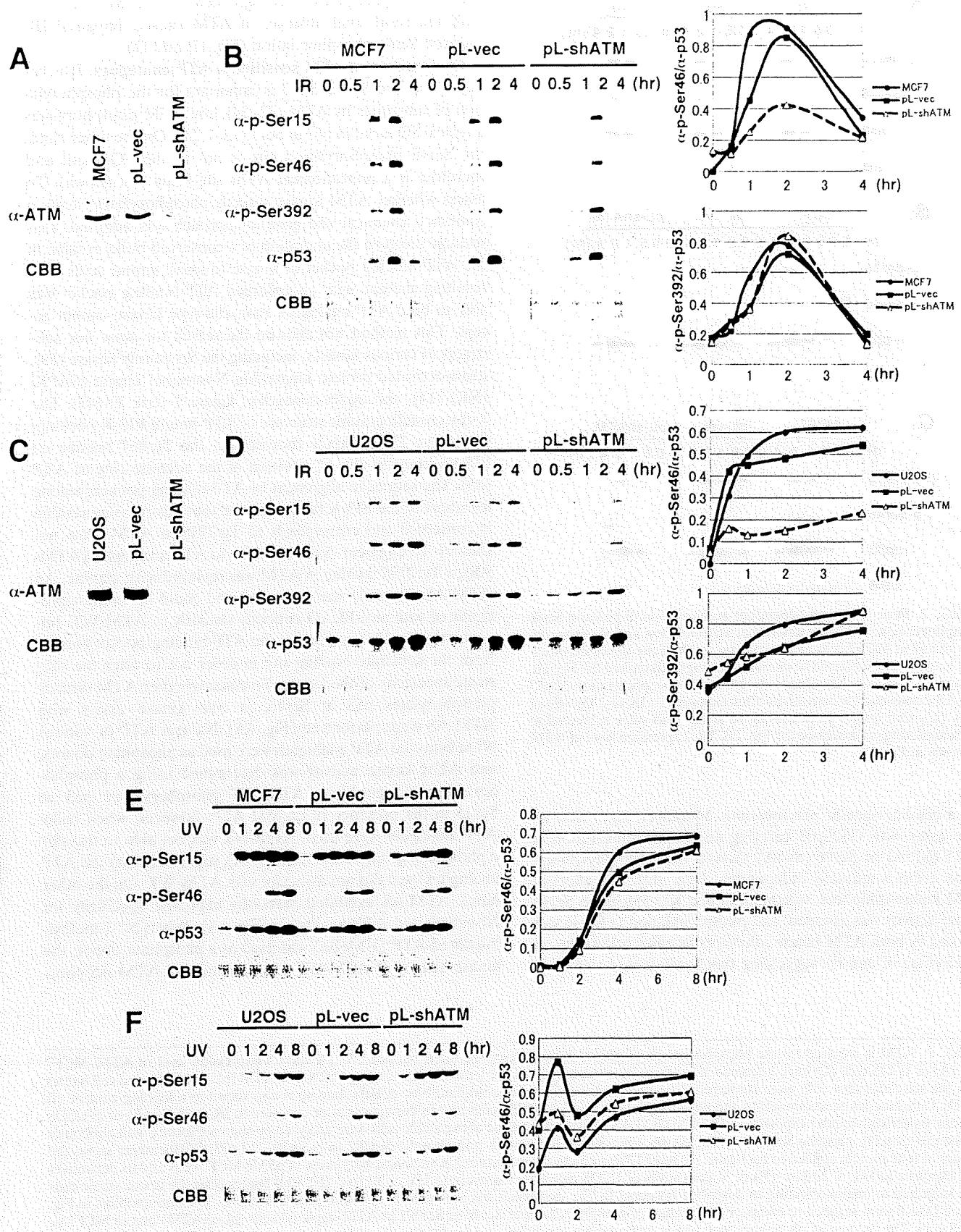

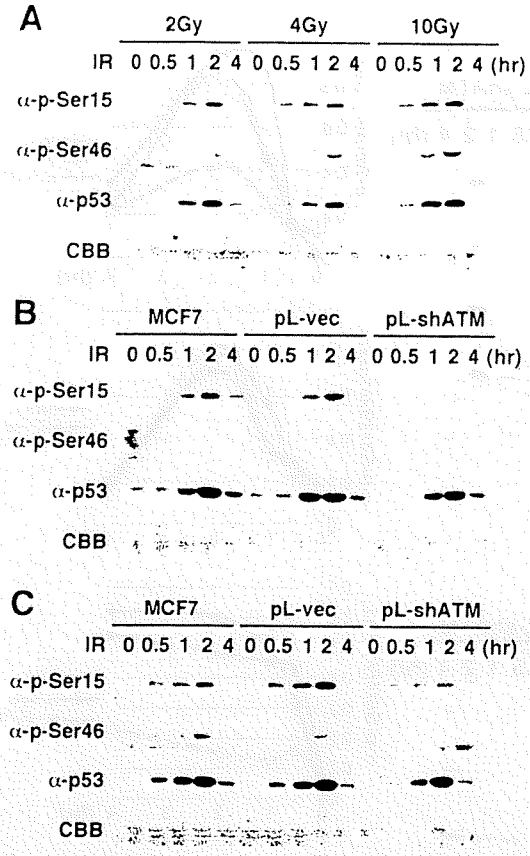

FIG. 2. Dose- and time-dependent accumulation of p53 and Ser46 phosphorylation. (A) Time kinetics of accumulation and phosphorylation of p53 in MCF7 cells after exposure to IR of the indicated doses. Cell lysates were subjected to immunoblotting as described for Fig. 1B. (B and C) Time kinetics of accumulation and phosphorylation of p53 in MCF7 cells and its derivatives after exposure to IR of 2 Gy (B) or 4 Gy (C). Cell lysates from the above stable cells were subjected to immunoblotting as described for Fig. 1B. The expression level of ATM is shown in Fig. 1A.

not a cell-line-specific phenomenon. Moreover, an *in vitro* kinase assay with GST-p53 carrying an alanine substitution at Ser15 (S15A) or Ser46 (S46A) showed that each phosphorylation event is mutually independent (Fig. 3D). The effect of ATM kinase inhibitors, wortmannin and KU-55933, on Ser46 kinase activity was assessed. p53 phosphorylation at Ser46 was blocked by both ATM kinase inhibitors as efficiently as that at Ser15 (Fig. 3E and F), suggesting that Ser46 kinase activity in the immunoprecipitate was dependent on ATM, consistent with the result that ablation of ATM caused impaired IR-induced Ser46 phosphorylation (Fig. 1B and D).

Construction of ATM sensitive to ATP analogues. It is believed that the S/T-Q motif is important for the phosphorylation of substrates by ATM (22, 34), and ATM phosphorylates a typical SQ motif in p53 at Ser15 (3, 7, 21). On the other hand, the Ser46 phosphorylation site is not in the SQ motif and therefore is a noncanonical ATM site (data not shown). To assess whether ATM kinase directly phosphorylates Ser46, a combined chemical and genetic approach was adopted. This strategy involved the alteration of a conserved bulky residue in the ATP-binding pocket of kinase to small amino acids. The resulting mutant with an enlarged ATP-binding pocket was able to bind ATP analogues that wild-type kinase cannot accept. This method has allowed the search for *bona fide* substrates of various kinases, including the Src family kinase (39), stress-activated protein kinase/Jun N-terminal kinase (SAPK/JNK) (14), and cyclin-dependent kinase 1 (cdk 1) (43). The X-ray crystallographic structure of ATP-bound PI3-Kγ belonging to the PI3-K family showed that the Tyr867 residue on PI3-Kγ contacts the N^6 position of the adenine ring of ATP (45). The sequence alignment of ATP-binding pockets among members of the PI3-K family showed that this tyrosine residue is conserved and corresponds to Tyr2755 in ATM (data not shown). To engineer ATM sensitive to ATP analogues (ATM-AS), a Tyr2755 residue in ATM was replaced with alanine. An ATM-AS molecule was expressed and could be immunoprecipitated with anti-FLAG antibody similarly to ATM-WT. Importantly, Tyr2755 is deep in the ATP-binding pocket and far from the substrate binding site in order not to alter the substrate specificity of the kinase. To assess whether ATM directly phosphorylates p53 at Ser46, *in vitro* kinase assays with ATM-AS were performed (Fig. 4A). Natural ATP or various N^6-substituted ATP analogues were used as phosphate donors, and ATM kinase activity was determined using a phospho-Ser15-specific antibody. ATM-WT phosphorylated p53 at Ser15 in the presence of natural ATP; however, when bulky ATP analogues were used, ATM-WT was not able to transfer a phosphate group to Ser15 (Fig. 4A), suggesting that the ATP analogues used did not associate with ATM-WT. On the other hand, ATM-AS exhibited markedly improved specificity for N^6-substituted ATP analogues (Fig. 4A). When N^6-1-methylbutylated-ATP (1-MeBu) was used as a phosphate donor, the kinase activity of ATM-WT was minimal and ATM-AS phos-

FIG. 1. ATM is required for the phosphorylation of p53 at Ser46 in response to IR but not UV. (A and C) Expression level of ATM. MCF7 cells (A) or U2OS cells (C) were infected with control lentiviruses (pL-vec) or lentiviruses encoding shRNA to ATM (pL-shATM), and cell lysates from the selected stable cells were subjected to immunoblotting. Coomassie brilliant blue (CBB) staining is also shown as a loading control. (B and D) Time kinetics of accumulation and phosphorylation of p53 in MCF7 cells and its derivatives after exposure to IR of 10 Gy (B) or in U2OS cells and its derivatives after exposure to IR of 20 Gy (D). Cell lysates from the above stable cells were analyzed by immunoblotting with antibodies against p53 (α-p53), phospho-Ser15 (α-p-Ser15), phospho-Ser46 (α-p-Ser46), and phospho-Ser392 (α-p-Ser392) of p53. CBB staining shows the amount of total protein applied to each lane. (E and F) Time kinetics of accumulation and phosphorylation of p53 in MCF7 cells and its derivatives after exposure to UV of 20 J/m^2 (E) or in derivatives of U2OS cells after exposure to UV of 30 J/m^2 (F). Cell lysates from the above stable cells were subjected to immunoblotting as described for panel B. The expression level of ATM is shown in panels A and C. The immunoblots in Fig. 1B and D to F were scanned to compare the amount of phosphorylation at Ser46 or Ser392 in ATM-depleted cells (pL-shATM) and in MCF7 or U2OS cells. The amount of phosphorylated p53 at each residue was calculated by dividing the value of phosphorylated p53 by that of total p53 at that time point.

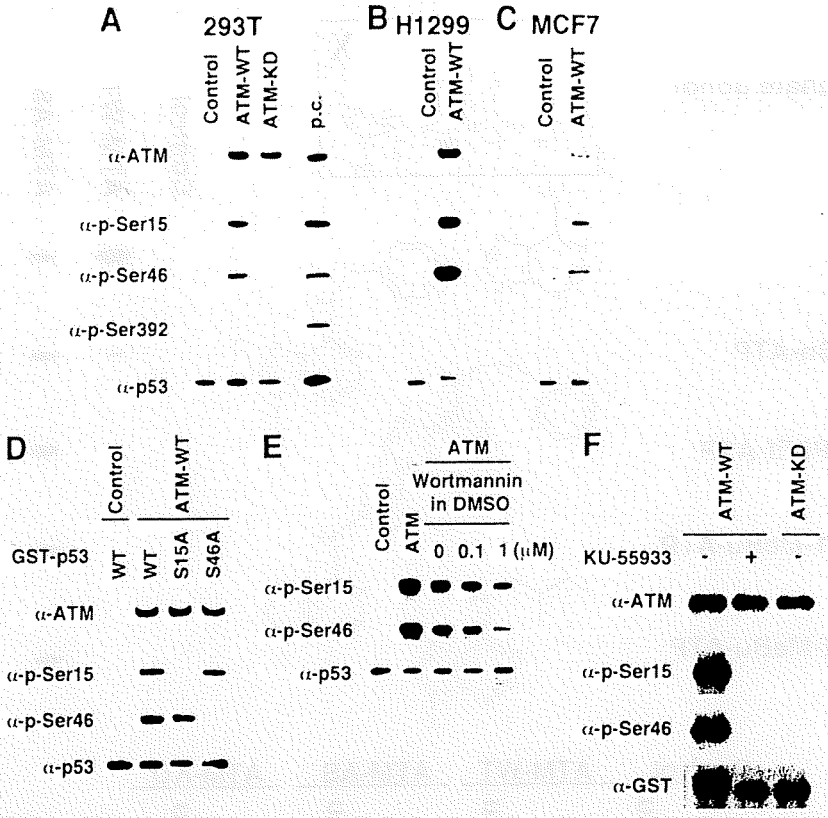

FIG. 3. ATM phosphorylates p53 fused to GST (GST-p53) at Ser46 *in vitro*. (A) Kinase activity of ATM. HEK 293T cells were transiently transfected with an empty vector (control) or an expression construct of FLAG-ATM wild-type (ATM-WT) or kinase-dead ATM (ATM-KD). The kinase activity of ATM purified with an anti-FLAG antibody was analyzed by an *in vitro* kinase assay using GST-p53 as a substrate. Phosphorylated p53 was detected by immunoblotting with the indicated antibodies. ATM in the reaction mixture was also detected by anti-ATM antibody. Cell lysates from MCF7 cells treated with 3 μM ADR are used for positive controls (p.c.) of antibodies. (B and C) Kinase activity of ATM in lysates from different cell lines. H1299 (B) or MCF7 (C) cells were transiently transfected with an empty vector (control) or an expression construct of FLAG-ATM-WT. The kinase activity of ATM purified with an anti-FLAG antibody was analyzed by an *in vitro* kinase assay using GST-p53 as a substrate. Phosphorylated p53 was detected by immunoblotting as described for panel A. (D) GST-p53 carrying an alanine substitution at Ser15 (S15A) or at Ser46 (S46A) was subjected to the *in vitro* kinase assay as in panel A. (E) Effect of an ATM kinase inhibitor on the Ser46 kinase activity of ATM. The *in vitro* kinase assay was performed as in panel A with different concentrations of wortmannin. DMSO, dimethyl sulfoxide. (F) Effect of KU-55933 on the Ser46 kinase activity of ATM. The *in vitro* kinase assay was performed as in panel A with or without 10 μM KU-55933. α, anti.

phorylated p53 at Ser15 more efficiently than ATM-WT (Fig. 4A, row IV).

Kinase domain of ATM directly phosphorylates Ser46 of p53. To explore whether ATM itself directly phosphorylates Ser46 on p53, *in vitro* kinase assays using ATM-AS and N^6-1-MeBu-ATP were performed. If ATM directly phosphorylates Ser46 on p53, ATM-AS would phosphorylate Ser46 as well as Ser15 with N^6-1-MeBu-ATP. If ATM activates a separate Ser46 kinase that is contained in the ATM immune complex, ATM-AS would phosphorylate Ser15 but not Ser46 with N^6-1-MeBu-ATP, as unmodified kinases cannot use ATP analogues as a phosphate donor. The *in vitro* kinase assay revealed that the phosphorylation pattern of Ser46 was quite similar to that of Ser15 (Fig. 4B). ATM-AS phosphorylated both serine residues more efficiently than normal ATP even when N^6-1-MeBu-ATP was used (Fig. 4B, lanes 8 and 9). In contrast, ATM-WT phosphorylated both Ser15 and Ser46 of p53 only in the presence of normal ATP (Fig. 4B, lanes 5 and 6). These phosphorylations were not due to contamination of ATP associated with the immunoprecipitates because the immunoprecipitate complex did not phosphorylate p53 in the absence of phosphate donors (Fig. 4B, lanes 1, 4, 7, and 10). These findings suggest that ATM itself directly phosphorylates Ser46 without any effector kinase.

ATM requires N- and C-terminal domains of p53 for Ser46 phosphorylation. To investigate how ATM phosphorylates a noncanonical target such as Ser46 on p53, the efficiency of Ser46 phosphorylation was analyzed using various deletion mutants of p53. The consensus sequences required for phosphorylation by ATM were identified using a short peptide library (22, 34). However, there is a possibility that ATM might require the whole structure of substrates for sufficient phosphorylation. Therefore, the phosphorylation efficiency between full-length p53 and a short peptide containing Ser15 or Ser46 was compared to evaluate whether Ser46 phosphorylation is a conformation-dependent event. ATM was able to phosphorylate Ser15 on short peptides as efficiently as full-length p53 (Fig. 5A, left). In contrast, no Ser46 phosphorylation was detected on a short peptide (Fig. 5A, right), indicating that the whole structure of p53 is required for Ser46 phosphorylation.

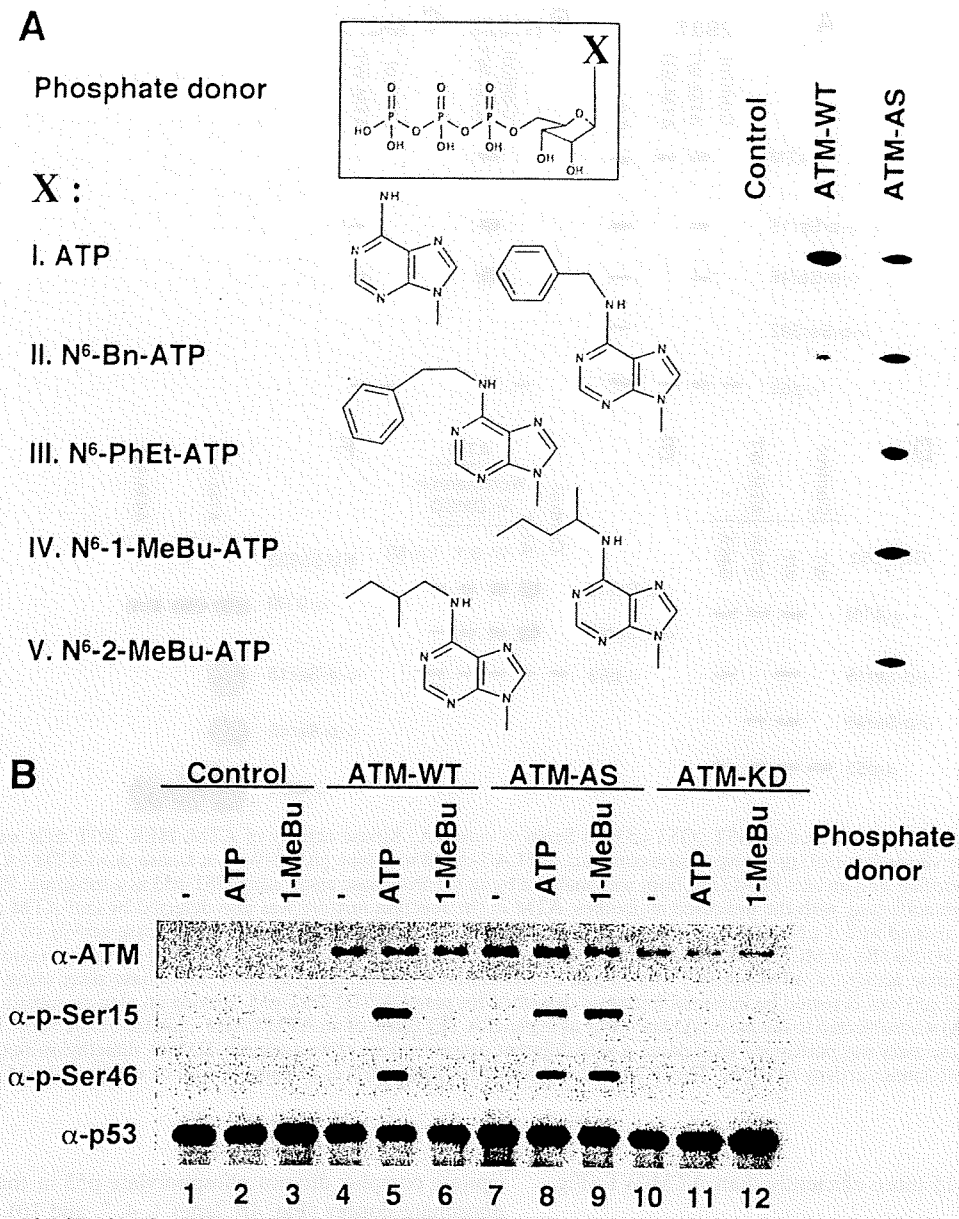

FIG. 4. ATM directly phosphorylates Ser46 of p53 using a mechanism different from that for Ser15. (A) Recombinant ATM was purified from 293T cells expressing FLAG-tagged ATM using anti-FLAG antibody and detected by immunoblotting with anti-ATM antibody. Kinase activity of ATM-WT or an ATM mutant sensitive to ATP analogues (ATM-AS and ATM-Y2755A) was measured by *in vitro* kinase assays using GST-p53. In this assay, natural ATP or various N^6-substituted ATP analogues (row I, ATP: row II, N^6-benzyl ATP [N^6-Bn-ATP]; row III, N^6-phenylethyl ATP [N^6-PhEt-ATP]; row IV, N^6-1-methylbutyl ATP [N^6-1-MeBu-ATP]; row V, N^6-2-methylbutyl ATP [N^6-2-MeBu-ATP]) were used as phosphate donors, and the kinase activity was determined using α-p-Ser15 of p53 antibody. (B) *In vitro* kinase assays of ATM-WT, ATM-AS, and ATM-KD using GST-p53 as the substrate. Immunoprecipitates from 293T cells transfected with empty vector (control) were also subjected to the same assay. ATP or N^6-1-MeBu-ATP (1-MeBu) was used as a phosphate donor for the kinase reaction. "−" indicates a sample without a phosphate donor in the reaction mixture. α, anti.

To exclude the possibility that Ser46 was not exposed because a small region of p53 was fused to a larger GST protein, *in vitro* kinase assays using chemically synthesized p53 peptide were performed (data not shown). Dot blot analysis showed that ATM did not phosphorylate short peptides containing Ser46 without GST (data not shown). Furthermore, antibodies specifically recognized chemically synthesized phosphorylated forms of corresponding short peptides (data not shown). Taken together, these data suggest that the entire p53 structure is required for Ser46 phosphorylation.

To map other regions that may be required for Ser46 phosphorylation, various deletion mutants of p53 were used (Fig. 5B). Deletion of the proline-rich (ΔPro) or C-terminal (ΔC) domains of p53 caused decreased Ser46 phosphorylation *in vitro* (Fig. 5C). In contrast, deletion of the N-terminal TAD1 domain had little or no effect on Ser46 phosphorylation.

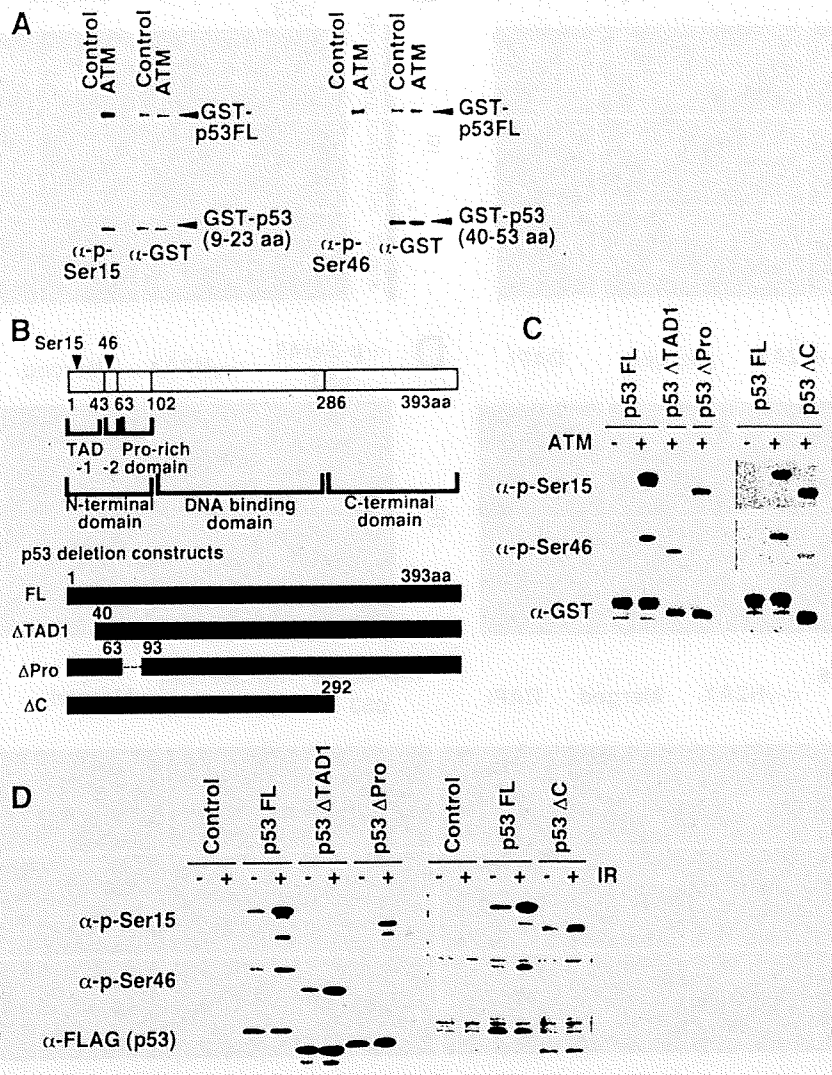

FIG. 5. ATM requires the whole structure of p53 for Ser46 phosphorylation. (A) Comparison experiments of phosphorylation by ATM between p53 full-length and short peptides containing Ser15 (left panel) or Ser46 (right panel) from p53. Full-length p53 and short peptides were produced as GST fusion proteins and used for *in vitro* kinase assay. To compare the phosphorylation efficiencies, full-length p53 and short peptides were mixed and the mixtures were subjected to immunoblotting with indicated antibodies. Specificity of α-p-Ser46 antibody was examined using peptides phosphorylated or not on Ser46 (data not shown). (B) Schematic representation of deletion mutants of p53. Various deletion mutants of p53 were used for the experiments shown in panels C and D. ΔTAD1 corresponds to the deletion of amino acids 1 to 39 of p53, ΔPro corresponds to the deletion of amino acids 64 to 92, and ΔC corresponds to the deletion of amino acids 292 to 393. (C and D) Phosphorylation of p53 deletion mutants *in vitro* (C) or *in vivo* (D). (C) *In vitro* kinase assays using deletion mutants of p53 fused to GST as the substrates. Immunoblotting with anti-GST antibody shows the amount of each substrate in the reaction mixture. (D) Deletion mutants of p53 were transiently expressed in H1299 cells, and at 24 h after transfection, cells were exposed to 0 Gy (−) or 10 Gy (+) of IR. The phosphorylation of p53 at 1 h after IR was detected by immunoblotting. α, anti.

To confirm the effect of the deletion of p53 on Ser46 phosphorylation *in vivo*, the deletion mutants of p53 used for *in vitro* kinase assays were expressed transiently in H1299 cells and the transfected cells were exposed to IR. The proline-rich and C-terminal domains were required for IR-dependent Ser46 phosphorylation (Fig. 5D), which was consistent with *in vitro* data shown above. These findings imply that the whole structure of p53 is required for Ser46 phosphorylation by ATM, although ATM is directed to Ser15 by amino acid sequences surrounding it.

ATM phosphorylates Ser46 of p53 at the sites of DSBs. After exposure to IR, activated ATM is recruited to DSBs and phosphorylates various substrates, including Chk2, SMC1, and H2AX (4, 24, 47). To investigate where ATM phosphorylates Ser46 on p53, antibodies specific for detection of Ser15- and Ser46-phosphorylated p53 were used for immunofluorescence analyses. The specificity of these antibodies was confirmed by immunofluorescence with p53 mutants bearing a mutation at Ser15 or at Ser46 and by immunoblotting with samples from cells with or without DNA damage (data not shown). Following exposure of cells to IR, p53 accumulated in the nuclei (Fig. 6A and B) and Ser15-phosphorylated p53 (Fig. 6A and C) exhibited a diffuse nuclear distribution. On the other hand, confocal immunofluorescent microscopic analyses with an an-

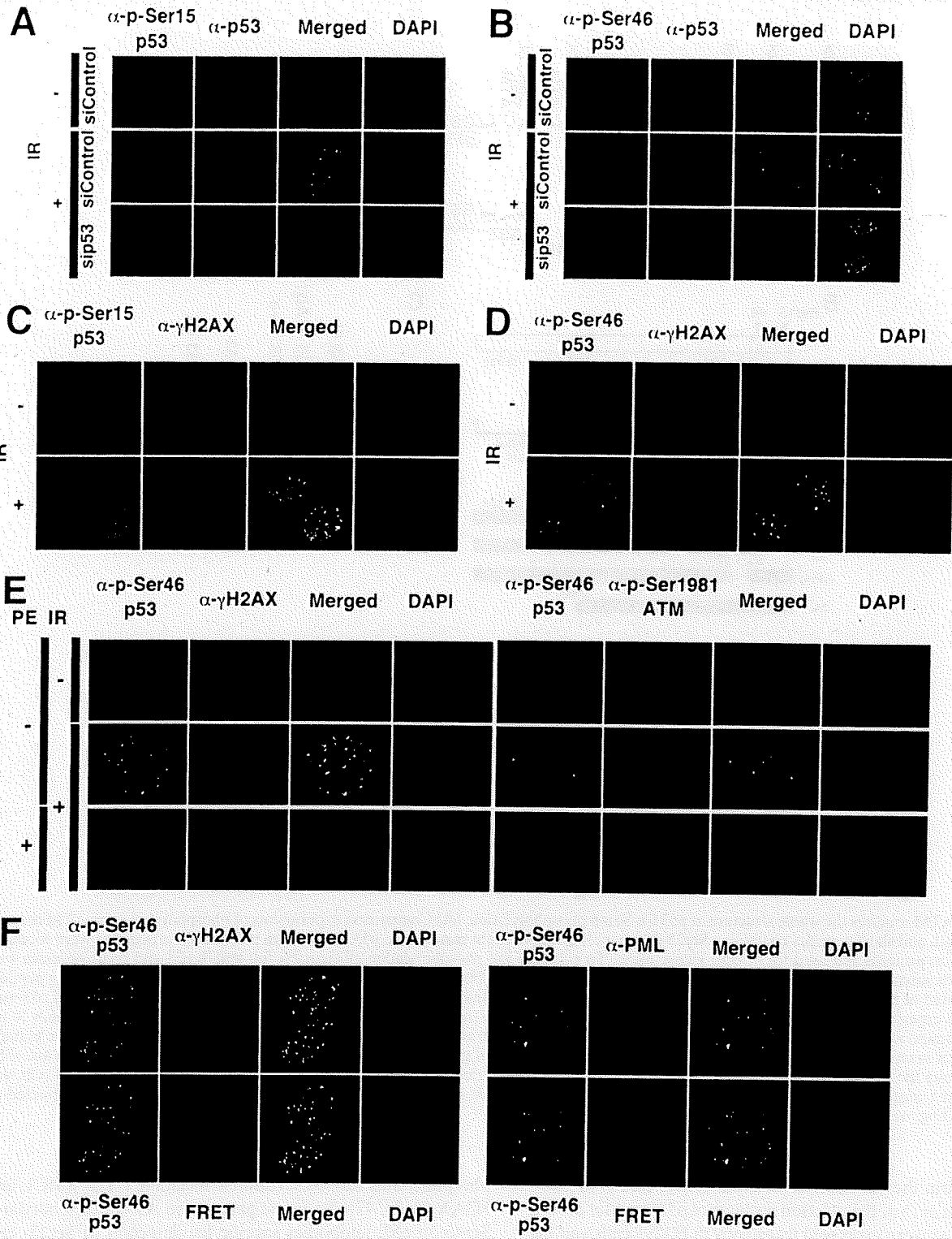

FIG. 6. Ser46, but not Ser15, of p53 is colocalized with activated ATM at DSB sites. (A and B) At 48 h after transfection with either control or p53 siRNA, MCF7 cells were exposed to 0 Gy (−) or 10 Gy (+) of IR and subjected to confocal immunofluorescent analysis at 30 min after irradiation. (A) Immunofluorescence with anti-phospho-Ser15-of-p53 (green) and anti-p53 (red) antibodies. (B) Immunofluorescence with anti-phospho-Ser46-of-p53 (green) and anti-p53 (red) antibodies. (C) Immunofluorescence with anti-phospho-Ser15-of-p53 (green) and anti-γ-H2AX (red) antibodies. (D) Immunofluorescence with anti-phospho-Ser46-of-p53 (green) and anti-γ-H2AX (red) antibodies. (E) Release of Ser46-phosphorylated p53 from chromatin by preextraction of a detergent prior to formaldehyde fixation. MCF7 cells were exposed to 0 Gy (−) or 10 Gy (+) of IR and subjected to confocal immunofluorescent analysis 30 min after irradiation. To assess whether activated ATM (Ser1981-phosphorylated ATM), Ser46-phosphorylated p53, or γ-H2AX is tightly associated with DSB, preextraction (PE) before fixation was performed. (F) Immunofluorescence with anti-phospho-Ser46-of-p53 (green) and anti-γ-H2AX or anti-PML (red) antibodies. Nuclei were stained with DAPI (blue). FRET signals occurring because of colocalization between Ser46-phosphorylated p53 and γ-H2AX or PML are shown (bottom panels).

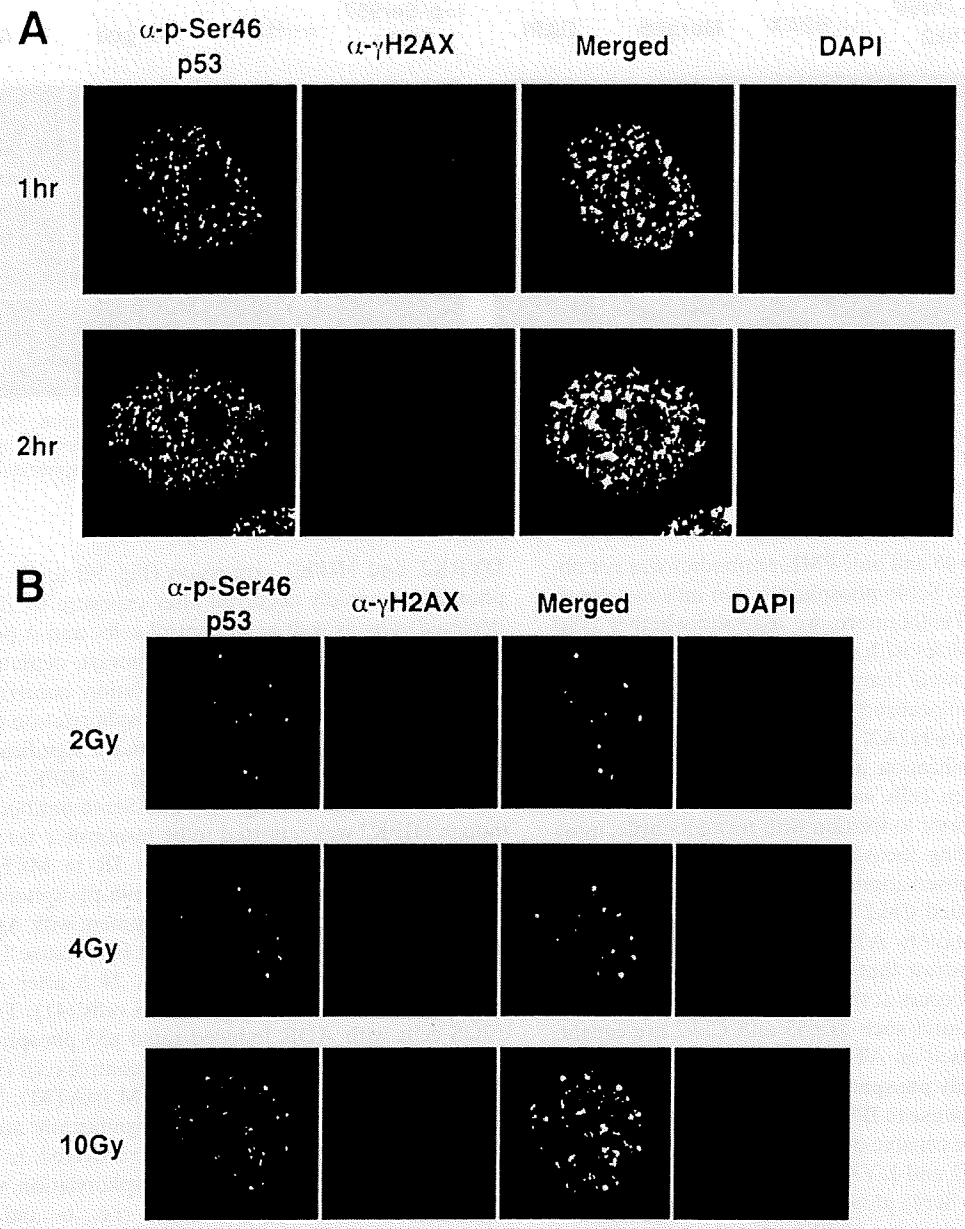

FIG. 7. Dose- and time-dependent accumulation of phospho-Ser46 foci. (A) MCF7 cells were exposed to 0 Gy (−) or 10 Gy (+) of IR and subjected to confocal immunofluorescent analysis at 1 or 2 h after irradiation. Immunofluorescence with anti-phospho-Ser46-of-p53 (green) and anti-γ-H2AX (red) antibodies. DAPI (blue) is also shown. (B) MCF7 cells were exposed to the indicated doses of IR and subjected to confocal immunofluorescent analysis at 30 min after irradiation. Immunofluorescence with anti-phospho-Ser46-of-p53 (green) and anti-γ-H2AX (red) antibodies. DAPI (blue) is also shown. α, anti.

tibody against phospho-Ser46 of p53 showed that Ser46-phosphorylated p53 was observed as foci (Fig. 6B) that partially colocalized with γ-H2AX (Fig. 6D) and Ser1981-phosphorylated ATM (Fig. 6E) but not the PML body (Fig. 6F), which has been known to form another nuclear focus. The foci of fluorescence signals from phospho-Ser46 of p53 in immunofluorescence were confirmed to be p53 itself by RNAi-directed ablation of p53 expression (Fig. 6A and B). Dose dependency of IR and time kinetic experiments showed that foci of phospho-Ser46 gradually increased in a dose-dependent manner and were observed even in cells irradiated at a lower dose (2 Gy, 30 min) (Fig. 7), at which Ser46 phosphorylation was not detected by immunoblot assays. The reason why phospho-Ser46 was not detected in immunoblots may be explained by Ser46-phosphorylated p53 in cells being diluted to perform immunoblot assays, whereas phospho-Ser46 concentrates as foci, subsequently observed by immunofluorescence. We also conducted fluorescence resonance energy transfer (FRET) experiments to show colocalization of phospho-Ser46 with DSB sites. As shown in Fig. 6F, a FRET signal was detected in immunofluorescence with anti-phospho-Ser46 and anti-γ-H2AX antibodies; whereas FRET from immunofluorescence

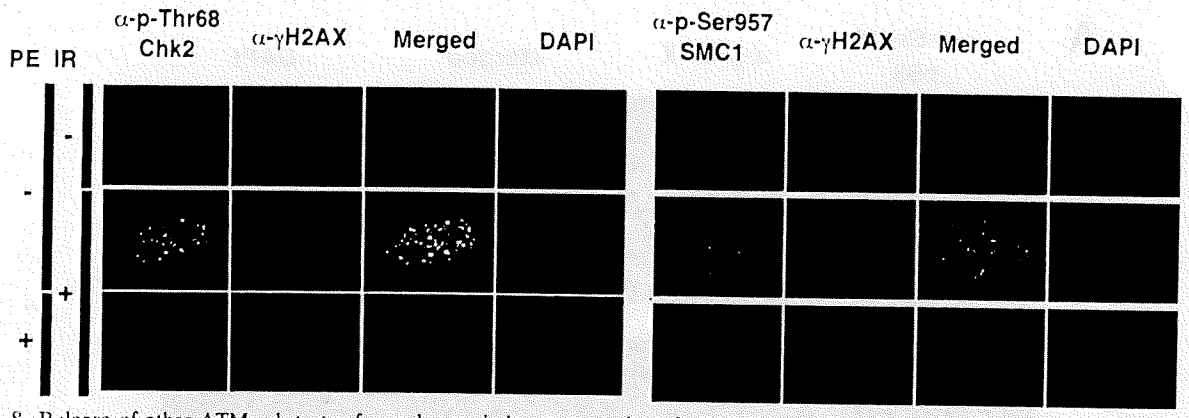

FIG. 8. Release of other ATM substrates from chromatin by preextraction of a detergent prior to formaldehyde fixation. MCF7 cells were exposed to 0 Gy (−) or 10 Gy (+) of IR and subjected to confocal immunofluorescent analysis 30 min after irradiation. To assess whether activated ATM (Ser1981-phosphorylated ATM) or protein phosphorylated by ATM (Thr68-phosphorylated Chk2, Ser957-phosphorylated SMC1, or γ-H2AX) is tightly associated with DSB, preextraction (PE) before fixation was performed. α, anti.

with anti-phospho-Ser46 and anti-PML antibodies was not observed, confirming that Ser46 phosphorylation indeed colocalized with DSB sites. Furthermore, we assessed whether DSB foci (γ-H2AX) colocalizes with Chk2 and SMC1. Immunofluorescent analyses showed that phosphoforms of Chk2 and SMC1 were partially colocalized with DSB foci (Fig. 8), as seen in phospho-Ser46-p53/γ-H2AX (Fig. 6D). We also assessed the effect of permeabilization of cells on the phospho-Ser46 focus formation. When cells were treated with a detergent (0.2% Triton X-100) prior to fixation with formaldehyde, most p53 molecules, including focus-associated p53, were washed out (Fig. 6E). These observations are similar to previous findings that focus-associated Chk2 immediately dissociates from chromatin after activation by ATM-mediated phosphorylation (4). These data demonstrate that Ser46 phosphorylation of p53 by IR-activated ATM occurs at the sites of DSBs, and it seems that some ATM substrates such as p53 and Chk2 are caught and immediately released on ATM-associated foci.

Ser46 is preferentially phosphorylated by ATM in the early inductive phase of response to DNA damage. Although several protein kinases that are capable of phosphorylating Ser46 have been identified, HIPK2 and DYRK2 are the most prominent kinases responsible for Ser46 phosphorylation (6, 9, 33, 41, 49). According to previous reports, HIPK2 phosphorylates Ser46 following exposure to UV (16), but it is controversial whether this kinase actually responds to double-strand breaks because Taira et al. have reported that HIPK2 is a specific kinase serving in a UV-mediated pathway (9, 16, 41). Another Ser46 kinase, DYRK2, phosphorylates following treatment with adriamycin (ADR), a radiomimetic DNA-damaging reagent (41). Although Ser46 phosphorylation observed in this report was obtained at late-phase response to DNA damage, a kinase responsible for Ser46 phosphorylation occurring at early-phase response to IR remains unidentified. Therefore, we next investigated whether ATM is required for Ser46 phosphorylation occurring at early-phase response to IR. In ATM-deficient AT2KY cells, Ser46 was not phosphorylated at early-phase response to DNA damage but became phosphorylated at late phase (Fig. 9A). To define the relation between ATM and other Ser46 kinases, Ser46 phosphorylation was assessed over 24 h under conditions of more than 80% reduction of ATM, DYRK2, and HIPK2 expression (Fig. 9B to E). Ser46 phosphorylation rapidly occurred after exposure to IR in HIPK2-depleted cells as well as in control cells, and it peaked at 2 h after IR treatment (Fig. 9C). In contrast, depletion of ATM causes decreased Ser46 phosphorylation occurring at early-phase response. However, Ser46 phosphorylation was detected after 24 h at a steady-state level and a significant effect on Ser46 phosphorylation by depletion of HIPK2 was not detected by immunoblotting with anti-Ser46 antibody. Thus, although HIPK2 was reported to be responsible for Ser46 phosphorylation observed at 24 h after IR in MCF7 cells (9), HIPK2 knockdown did not alter Ser46 phosphorylation (Fig. 9C). Damage response following treatment with ADR was also assessed using siRNAs (Fig. 9D and E) because DYRK2 was reported to phosphorylate Ser46 at 24 h after exposure to ADR in human osteosarcoma U2OS cells (41). Treatment of U2OS cells with ADR induced rapid p53 phosphorylation at Ser46, and it continued over 24 h in control cells (Fig. 9E). In cells transfected with siRNA for ATM (siATM), Ser46 phosphorylation induced by ADR was significantly attenuated in early phase (Fig. 9E), but it gradually recovered. In contrast, in cells devoid of DYRK2, Ser46 phosphorylation was not affected during early response times (i.e., 6- and 12-h time points), but levels decreased by 24 h as expected (Fig. 9E). Again, HIPK2 knockdown using siRNA did not alter Ser46 phosphorylation and had only a marginal effect on Ser46 phosphorylation (Fig. 9E). On the other hand, upon UV treatment, Ser46 phosphorylation is severely affected by HIPK2 knockdown (Fig. 9F), suggesting that HIPK2 seems to be a kinase directed by UV irradiation, at least under our conditions. These observations suggest that ATM is selectively responsible for Ser46 phosphorylation in early-inductive-phase response to DSBs.

DISCUSSION

Here, we found that Ser46 on p53 is directly phosphorylated by ATM in response to IR. Although ATM preferentially phosphorylates S/T-Q sequences (22, 34), the current experiments revealed that Ser46 is phosphorylated by ATM in a conformation-dependent manner, although this site is an S-P

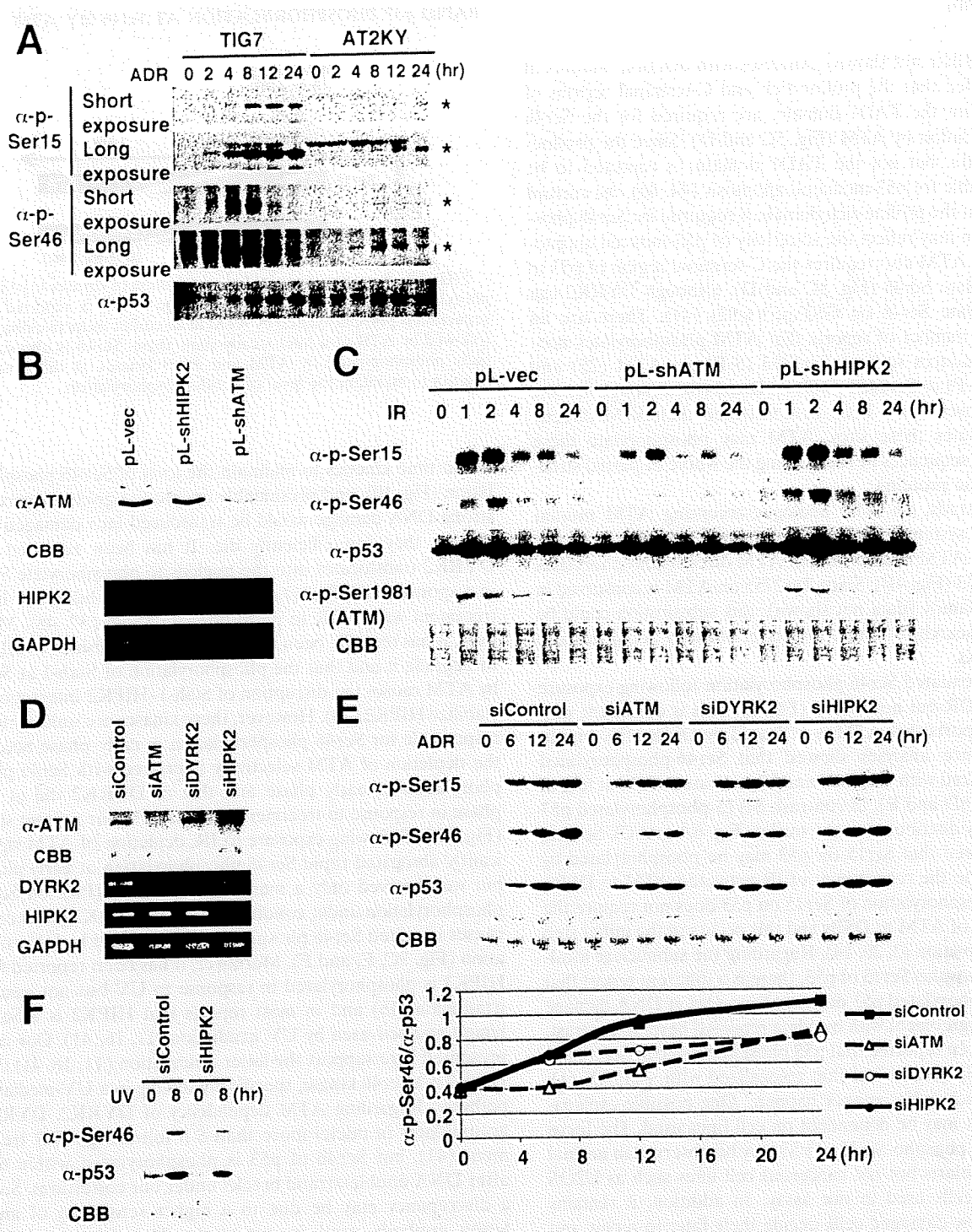

FIG. 9. ATM preferentially phosphorylates p53 at Ser46 in early-phase response to DSBs. (A) Time kinetics of accumulation and phosphorylation of p53 in human fibroblast TIG7 cells or AT2KY cells, human fibroblast cells derived from an A-T patient, treated with 3 μM ADR for indicated periods. Cell lysates were assayed as described for Fig. 1B. Stars indicate bands specific to antibodies. (B and C) ATM is required for Ser46 phosphorylation of p53 in early-phase response to IR. (B) Expression of ATM or HIPK2 in MCF7 cells infected with control lentiviruses (pL-control) or lentiviruses encoding shRNA to HIPK2 (pL-shHIPK2) or ATM (pL-shATM). Expression of ATM was examined by immunoblotting. Expression of HIPK2 was examined by RT-PCR. Coomassie brilliant blue (CBB) staining and RT-PCR of GAPDH are shown for loading controls. (C) Time kinetics of accumulation and phosphorylation of p53 after cellular exposure to IR of 10 Gy. Cell lysates were assayed as described for Fig. 1B. (D to F) ATM is required for Ser46 phosphorylation of p53 in early-phase response to ADR. (D) Expression of ATM, DYRK2, or HIPK2 in U2OS cells transfected with either control siRNA (siControl), siRNA to ATM (siATM), DYRK2 (siDYRK2), or HIPK2 (siHIPK2). The expression level of ATM was determined by immunoblotting, and expression levels of DYRK2 and HIPK2 were determined by RT-PCR. As loading controls, CBB staining and RT-PCR of GAPDH are also indicated. (E and F) Accumulation of p53 and Ser46 phosphorylation occurred in early-phase response to ADR or UV irradiation. U2OS cells transfected with indicated siRNAs were treated with 0.5 μM ADR (E) or 30 J/m^2 UV (F) for indicated periods, and cell lysates were assayed as described in Fig. 1B. The amount of Ser46-phosphorylated p53 was calculated by dividing the value of phosphorylated p53 by that of total p53 at that time point.

sequence (data not shown). Analyses with deletion mutants of p53 revealed that the proline-rich and C-terminal regions of p53, but not the TAD1 domain, are required for the Ser46 phosphorylation by ATM (Fig. 5C and D). Since the proline-rich domain, but not the TAD1 domain, is reported to be indispensable for p53-mediated apoptosis (44, 46), the current finding that the proline-rich domain is required for Ser46 phosphorylation may reflect the selectivity of p53-induced apoptosis. Again, ATM also requires the C-terminal region of p53 to phosphorylate Ser46 (Fig. 5C and D), although DYRK2 can phosphorylate Ser46 on GST-p53(1-92) (41). There are an increasing number of reports that ATM phosphorylates non-S/T-Q sequences such as Ser1893 (S-E) on ATM (25) and Ser1189 (S-P) or Ser1452 (S-G) on Brca1 (8), although in none of these cases has it been demonstrated that ATM directly phosphorylates these sites. ATM may phosphorylate these non-S/T-Q sequences by recognizing the whole or partial structure of these proteins.

In this study, an ATP analogue-accepting ATM mutant (ATM-AS) system was constructed by alanine substitution for Tyr2755 on ATM to confirm that ATM directly phosphorylates Ser46 on p53 (Fig. 4B). Since Tyr2755 on ATM is conserved in the PI3-K family (data not shown), this substitution could be applied to search for direct targets of not only ATM but also other PI3-Ks.

ATM attenuated Ser46 phosphorylation following exposure to IR or ADR but not to UV (Fig. 1). This is consistent with previous reports that ATM is activated by DSBs (19). Immunofluorescence analyses showed that Ser46-phosphorylated p53 colocalized with γ-H2AX and IR-activated ATM at foci of DSBs (Fig. 6D and E); in contrast, Ser15-phosphorylated p53 was diffusely distributed in the nuclei (Fig. 6A and C). Several groups showed that Ser15 on p53 may be phosphorylated by ATM prior to the recruitment of IR-activated ATM to DSBs, because phosphorylation of Ser15 on p53 does not require the recruitment of ATM to DSBs and this occurs in the initial step of ATM activation (2, 20, 24). Regarding the subnuclear localization of phospho-Ser15 of p53, there is a different report that Ser15-phosphorylated p53 does not form foci at DNA damage sites (4), in agreement with our data reported here. In contrast, it has also been reported that p53 phosphorylated at Ser15, but not bulk p53, formed foci that colocalized with γ-H2AX (1). Why does such a discrepancy happen? One possible explanation is that it may be dependent on cell lines used. The focus formation of phospho-Ser15 of p53 may be observed in normal diploid fibroblasts but not cancerous cell lines such as U2OS and MCF7 cells used in our assay. In addition, it remains enigmatic how damaged cells decide their fate: to repair and live or to die. The current observation that Ser46 is phosphorylated by ATM at DSBs may explain the previous report that phosphorylation of Ser15 on p53 is much more sensitive to cell damage and occurs rapidly compared to phosphorylation at Ser46, which is important for induction of apoptosis (33).

Time course experiments revealed that depletion of ATM selectively interfered with Ser46 phosphorylation at early phase (Fig. 9C and E). In response to IR, Ser15 is sequentially phosphorylated by ATM at an earlier inductive phase and by an A-T and Rad3-related (ATR) kinase at a later steady-state phase (Fig. 10) (42). Our data also suggest that Ser46 is sequentially phosphorylated by ATM and other kinases at different time kinetics to maintain the level of Ser46 phosphorylation (Fig. 10), and presumably apoptotic signals triggered by strong DNA damage would be transduced into damaged cells so that they can efficiently die. It has been reported that DYRK2 translocates into the nucleus to phosphorylate Ser46 in response to ADR (41) and that HIPK2 is stabilized by IR or treatment with ADR to phosphorylate Ser46 (37, 48). Moreover, it has recently been reported that Siah-1 binds to HIPK2 to degrade it and that the phosphorylation of Siah-1 at Ser19 by ATM causes the disruption of Siah-1–HIPK2 interaction to stabilize HIPK2 (48). However, these kinases are unlikely to be responsible for Ser46 phosphorylation in early phase because the depletion of ATM selectively interfered with Ser46 phosphorylation at early phase and that of DYRK2 did at late phase in response to treatment with ADR in our present study (Fig. 9E). Following exposure to IR, depletion of ATM significantly abrogated rapid Ser46 phosphorylation at early phase, but we observed only a marginal effect of HIPK2 on Ser46 phosphorylation under conditions in which HIPK2 knockdown causes impaired Ser46 phosphorylation directed by UV irradiation (Fig. 9C, E, and F). Moreover, it has been reported that HIPK2 is phosphorylated in response to UV but not gamma irradiation (16) and in most reports that HIPK2 is a Ser46 kinase and activated by UV irradiation (11, 16, 41). Our data presented here support the latter observation (11, 16, 41) that HIPK2 is a Ser46 kinase, specifically serving in a UV-mediated pathway. Regarding ATM dependency of DYRK2, DYRK2 accumulates in nuclei more than 8 h following ADR treatment (41), but Ser46 of p53 is phosphorylated within 6 h after DNA double-strand breaks under our conditions. Such a discrepancy may be due to a higher sensitivity of anti-Ser46 antibody used in our study. Therefore, probably, DYRK2 seems to be dependent on ATM and may be required for Ser46 phosphorylation occurring at late-phase response of DNA double-strand breaks.

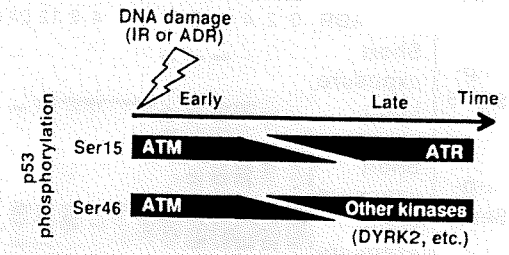

FIG. 10. A proposed model for contribution of kinases to p53 phosphorylation. In response to DNA damage, Ser15 is reported to be sequentially phosphorylated by ATM at an earlier inductive phase and followed by ATR at a later steady-state phase. Ser46 is also sequentially phosphorylated by ATM and other kinases at different time kinetics to maintain the level of Ser46 phosphorylation.

In our present study, IR-activated ATM is partially colocalized with Ser46-phosphorylated p53 in response to DNA damage, suggesting that p53 phosphorylation at Ser46 is required to trigger early apoptotic signals to damaged cells. The reason why Ser46-phosphorylated p53 is recruited to DSB sites is still unclear. It has been reported that Chk2 is phosphorylated by ATM near DSB sites and that activated Chk2 releases from DSB sites to function during G_1 and G_2 checkpoints (30, 32). Similarly, activated ATM phosphorylates p53 at Ser46 near

DSB sites and Ser46-phosphorylated p53 may release from DSB sites to promote transcription of proapoptotic genes. Under various stresses, including UV and IR, DYRK2 and HIPK2 may work together with ATM to phosphorylate p53 at Ser46, leading to apoptosis to ensure that severely damaged cells are completely killed, though further investigations are needed to elucidate the molecular mechanisms of ATM-triggered p53-mediated apoptosis.

In conclusion, our present study strongly supports the idea that ATM directly phosphorylates p53 at Ser46 and is required for Ser46 phosphorylation occurring in early-phase DNA damage response. The direct link of ATM to Ser46 phosphorylation of p53 provides new insights into ATM-mediated p53-dependent apoptosis, though it cannot be ruled out that ATM may require adaptor proteins for Ser46 phosphorylation near DSB sites to facilitate its phosphorylation. Here, we show that ATM is likely to directly phosphorylate Ser46 of p53, but the kinase activity for Ser46 may be dependent on unidentified posttranslational modifications of ATM in response to severe DNA damage. In addition, it is quite difficult to determine *bona fide in vivo* kinases responsible for Ser46, so we cannot exclude the possibility that ATM is indirectly involved in the phosphorylation of Ser 46. Therefore, further studies are required to clarify whether ATM is a *bona fide in vivo* kinase responsible for Ser46 phosphorylation.

ACKNOWLEDGMENTS

We are grateful to Michael B. Kastan (St. Jude Children's Research Hospital) for the expression vector for FLAG-tagged ATM wild type. We also thank Kiyotsugu Yoshida (Tokyo Medical and Dental University, Japan) for valuable discussions with respect to DYRK2 and Kyoko Fujinaka (National Cancer Center Research Institute, Japan) for technical assistance.

This work was supported by a Grant-in-Aid for Scientific Research on Priority Areas (17013088) (to Y.T. and M.E.); SORST, Japan Science and Technology (to Y.T.); and a grant from the Takeda Science Foundation (to M.E.).

REFERENCES

1. **Al Rashid, S. T., G. Dellaire, A. Cuddihy, F. Jalali, M. Vaid, C. Coackley, M. Folkard, Y. Xu, B. P. Chen, D. J. Chen, L. Lilge, K. M. Prise, D. P. Bazett Jones, and R. G. Bristow.** 2005. Evidence for the direct binding of phosphorylated p53 to sites of DNA breaks in vivo. Cancer Res. **65**:10810–10821.
2. **Bakkenist, C. J., and M. B. Kastan.** 2003. DNA damage activates ATM through intermolecular autophosphorylation and dimer dissociation. Nature **421**:499–506.
3. **Banin, S., L. Moyal, S. Shieh, Y. Taya, C. W. Anderson, L. Chessa, N. I. Smorodinsky, C. Prives, Y. Reiss, Y. Shiloh, and Y. Ziv.** 1998. Enhanced phosphorylation of p53 by ATM in response to DNA damage. Science **281**:1674–1677.
4. **Bekker-Jensen, S., C. Lukas, R. Kitagawa, F. Melander, M. B. Kastan, J. Bartek, and J. Lukas.** 2006. Spatial organization of the mammalian genome surveillance machinery in response to DNA strand breaks. J. Cell Biol. **173**:195–206.
5. **Bourdon, J. C., V. D. Laurenzi, G. Melino, and D. Lane.** 2003. p53: 25 years of research and more questions to answer. Cell Death Differ. **10**:397–399.
6. **Bulavin, D. V., S. Saito, M. C. Hollander, K. Sakaguchi, C. W. Anderson, E. Appella, and A. J. J. Fornace.** 1999. Phosphorylation of human p53 by p38 kinase coordinates N-terminal phosphorylation and apoptosis in response to UV radiation. EMBO J. **18**:6845–6854.
7. **Canman, C. E., D. S. Lim, K. A. Cimprich, Y. Taya, K. Tamai, K. Sakaguchi, E. Appella, M. B. Kastan, and J. D. Siliciano.** 1998. Activation of the ATM kinase by ionizing radiation and phosphorylation of p53. Science **281**:1677–1679.
8. **Cortez, D., Y. Wang, J. Qin, and S. J. Elledge.** 1999. Requirement of ATM-dependent phosphorylation of brca1 in the DNA damage response to double-strand breaks. Science **286**:1162–1166.
9. **Dauth, I., J. Kruger, and T. G. Hofmann.** 2007. Homeodomain-interacting protein kinase 2 is the ionizing radiation-activated p53 serine 46 kinase and is regulated by ATM. Cancer Res. **67**:2274–2279.
10. **Di Stefano, V., C. Rinaldo, A. Sacchi, S. Soddu, and G. D'Orazi.** 2004. Homeodomain-interacting protein kinase-2 activity and p53 phosphorylation are critical events for cisplatin-mediated apoptosis. Exp. Cell Res. **293**:311–320.
11. **D'Orazi, G., B. Cecchinelli, T. Bruno, I. Manni, Y. Higashimoto, S. Saito, M. Gostissa, S. Coen, A. Marchetti, G. Del Sal, G. Piaggio, M. Fanciulli, E. Appella, and S. Soddu.** 2002. Homeodomain-interacting protein kinase-2 phosphorylates p53 at Ser 46 and mediates apoptosis. Nat. Cell Biol. **4**:11–19.
12. **Endo, Y., A. Sugiyama, S. A. Li, K. Ohmori, H. Ohata, Y. Yoshida, M. Shibuya, K. Takei, M. Enari, and Y. Taya.** 2008. Regulation of clathrin-mediated endocytosis by p53. Genes Cells **13**:375–386.
13. **Giaccia, A. J., and M. B. Kastan.** 1998. The complexity of p53 modulation: emerging patterns from divergent signals. Genes Dev. **12**:2973–2983.
14. **Habelhah, H., K. Shah, L. Huang, A. L. Burlingame, K. M. Shokat, and Z. Ronai.** 2001. Identification of new JNK substrate using ATP pocket mutant JNK and a corresponding ATP analogue. J. Biol. Chem. **276**:18090–18095.
15. **Harris, S. L., and A. J. Levine.** 2005. The p53 pathway: positive and negative feedback loops. Oncogene **24**:2899–2908.
16. **Hofmann, T. G., A. Moller, H. Sirma, H. Zentgraf, Y. Taya, W. Droge, H. Will, and M. L. Schmitz.** 2002. Regulation of p53 activity by its interaction with homeodomain-interacting protein kinase-2. Nat. Cell Biol. **4**:1–10.
17. **Hofmann, T. G., N. Stollberg, M. L. Schmitz, and H. Will.** 2003. HIPK2 regulates transforming growth factor-beta-induced c-Jun NH(2)-terminal kinase activation and apoptosis in human hepatoma cells. Cancer Res. **63**: 8271–8277.
18. **Ichwan, S. J., S. Yamada, P. Sumrejkanchanakij, E. Ibrahim-Auerkari, K. Eto, and M. A. Ikeda.** 2006. Defect in serine 46 phosphorylation of p53 contributes to acquisition of p53 resistance in oral squamous cell carcinoma cells. Oncogene **25**:1216–1224.
19. **Ismail, I. H., S. Nyström, J. Nygren, and O. Hammarsten.** 2005. Activation of ataxia telangiectasia mutated by DNA strand break-inducing agents correlates closely with the number of DNA double strand breaks. J. Biol. Chem. **280**:4649–4655.
20. **Kanu, N., and A. Behrens.** 2007. ATMIN defines an NBS1-independent pathway of ATM signalling. EMBO J. **26**:2933–2941.
21. **Khanna, K. K., K. E. Keating, S. Kozlov, S. Scott, M. Gatei, K. Hobson, Y. Taya, B. Gabrielli, D. Chan, S. P. Lees-Miller, and M. F. Lavin.** 1998. ATM associates with and phosphorylates p53: mapping the region of interaction. Nat. Genet. **20**:398–400.
22. **Kim, S. T., D. S. Lim, C. E. Canman, and M. B. Kastan.** 1999. Substrate specificities and identification of putative substrates of ATM kinase family members. J. Biol. Chem. **274**:37538–37543.
23. **Kinoshita, A., H. Fukumoto, T. Shah, C. M. Whelan, M. C. Irizarry, and B. T. Hyman.** 2003. Demonstration by FRET of BACE interaction with the amyloid precursor protein at the cell surface and in early endosomes. J. Cell Sci. **116**:3339–3346.
24. **Kitagawa, R., C. J. Bakkenist, P. J. McKinnon, and M. B. Kastan.** 2004. Phosphorylation of SMC1 is a critical downstream event in the ATM-NBS1-BRCA1 pathway. Genes Dev. **18**:1423–1438.
25. **Kozlov, S. V., M. E. Graham, C. Peng, P. Chen, P. J. Robinson, and M. F. Lavin.** 2006. Involvement of novel autophosphorylation sites in ATM activation. EMBO J. **25**:3504–3514.
26. **Lavin, M. F., and Y. Shiloh.** 1997. The genetic defect in ataxia-telangiectasia. Annu. Rev. Immunol. **15**:177–202.
27. **Li, X., P. Dumont, A. Della Pietra, C. Shetler, and M. E. Murphy.** 2005. The codon 47 polymorphism in p53 is functionally significant. J. Biol. Chem. **280**:24245–24251.
28. **Lu, H., Y. Taya, M. Ikeda, and A. J. Levine.** 1998. Ultraviolet radiation, but not gamma radiation or etoposide-induced DNA damage, results in the phosphorylation of the murine p53 protein at serine-389. Proc. Natl. Acad. Sci. U. S. A. **95**:6399–6402.
29. **Matsuoka, S., B. A. Ballif, A. Smogorzewska, E. R. McDonald III, K. E. Hurov, J. Luo, C. E. Bakalarski, Z. Zhao, N. Solimini, Y. Lerenthal, Y. Shiloh, S. P. Gygi, and S. J. Elledge.** 2007. ATM and ATR substrate analysis reveals extensive protein networks responsive to DNA damage. Science **316**:1160–1166.
30. **Matsuoka, S., G. Rotman, A. Ogawa, Y. Shiloh, K. Tamai, and S. J. Elledge.** 2000. Ataxia telangiectasia-mutated phosphorylates Chk2 in vivo and in vitro. Proc. Natl. Acad. Sci. U. S. A. **97**:10389–10394.
31. **Meek, D. W., and C. W. Anderson.** 2009. Posttranslational modification of p53: cooperative integrators of function. Cold Spring Harbor Perspect. Biol. **1**:a000950.
32. **Melchionna, R., X. B. Chen, A. Blasina, and C. H. McGowan.** 2000. Threonine 68 is required for radiation-induced phosphorylation and activation of Cds1. Nat. Cell Biol. **2**:762–765.
33. **Oda, K., H. Arakawa, T. Tanaka, K. Matsuda, C. Tanikawa, T. Mori, H. Nishimori, K. Tamai, T. Tokino, Y. Nakamura, and Y. Taya.** 2000. p53AIP1, a potential mediator of p53-dependent apoptosis, and its regulation by Ser-46-phosphorylated p53. Cell **102**:849–862.
34. **O'Neill, T., A. J. Dwyer, Y. Ziv, D. W. Chan, S. P. Lees-Miller, R. H. Abraham, J. H. Lai, D. Hill, Y. Shiloh, L. C. Cantley, and G. A. Rathbun.**

2000. Utilization of oriented peptide libraries to identify substrate motifs selected by ATM. J. Biol. Chem. 275:22719–22727.
35. **Oren, M.** 2003. Decision making by p53: life, death and cancer. Cell Death Differ. 10:431–442.
36. **Prives, C.** 1998. Signaling to p53: breaking the MDM2-p53 circuit. Cell 95:5–8.
37. **Rinaldo, C., A. Prodosmo, F. Mancini, S. Iacovelli, A. Sacchi, F. Moretti, and S. Soddu.** 2007. MDM2-regulated degradation of HIPK2 prevents p53Ser46 phosphorylation and DNA damage-induced apoptosis. Mol. Cell 25:739–750.
38. **Saito, S., A. A. Goodarzi, Y. Higashimoto, Y. Noda, S. P. Lees-Miller, E. Appella, and C. W. Anderson.** 2002. ATM mediates phosphorylation at multiple p53 sites, including Ser(46), in response to ionizing radiation. J. Biol. Chem. 277:12491–12494.
39. **Shah, K., Y. Liu, C. Deirmengian, and K. M. Shokat.** 1997. Engineering unnatural nucleotide specificity for Rous sarcoma virus tyrosine kinase to uniquely label its direct substrates. Proc. Natl. Acad. Sci. U. S. A. 94:3565–3570.
40. **Shieh, S. Y., M. Ikeda, Y. Taya, and C. Prives.** 1997. DNA damage-induced phosphorylation of p53 alleviates inhibition by MDM2. Cell 91:325–334.
41. **Taira, N., K. Nihira, T. Yamaguchi, Y. Miki, and K. Yoshida.** 2007. DYRK2 is targeted to the nucleus and controls p53 via Ser46 phosphorylation in the apoptotic response to DNA damage. Mol. Cell 25:725–738.
42. **Tibbetts, R. S., K. M. Brumbaugh, J. M. Williams, J. N. Sarkaria, W. A. Cliby, S. Y. Shieh, Y. Taya, C. Prives, and R. T. Abraham.** 1999. A role for ATR in the DNA damage-induced phosphorylation of p53. Genes Dev. 13:152–157.
43. **Ubersax, J. A., E. L. Woodbury, P. N. Quang, M. Paraz, J. D. Blethrow, K. Shah, K. M. Shokat, and D. O. Morgan.** 2003. Targets of the cyclin-dependent kinase Cdk1. Nature 425:859–864.
44. **Venot, C., M. Maratrat, C. Dureuil, E. Conseiller, L. Bracco, and L. Debussche.** 1998. The requirement for the p53 proline-rich functional domain for mediation of apoptosis is correlated with specific PIG3 gene transactivation and with transcriptional repression. EMBO J. 17:4668–4679.
45. **Walker, E. H., M. E. Pacold, O. Perisic, L. Stephens, P. T. Hawkins, M. P. Wymann, and R. L. Williams.** 2000. Structural determinants of phosphoinositide 3-kinase inhibition by wortmannin, LY294002, quercetin, myricetin, and staurosporine. Mol. Cell 6:909–919.
46. **Walker, K. K., and A. J. Levine.** 1996. Identification of a novel p53 functional domain that is necessary for efficient growth suppression. Proc. Natl. Acad. Sci. U. S. A. 93:15335–15340.
47. **Ward, I. M., X. Wu, and J. Chen.** 2001. Threonine 68 of Chk2 is phosphorylated at sites of DNA strand breaks. J. Biol. Chem. 276:47555–47558.
48. **Winter, M., D. Sombroek, I. Dauth, J. Moehlenbrink, K. Scheuermann, J. Crone, and T. G. Hofmann.** 2008. Control of HIPK2 stability by ubiquitin ligase Siah-1 and checkpoint kinases ATM and ATR. Nat. Cell Biol. 10:812–824.
49. **Yoshida, K., H. Liu, and Y. Miki.** 2006. Protein kinase C delta regulates Ser46 phosphorylation of p53 tumor suppressor in the apoptotic response to DNA damage. J. Biol. Chem. 281:5734–5740.

doi:10.1016/j.jmb.2009.09.029 J. Mol. Biol. (2009) 394, 460–471

JMB

Available online at www.sciencedirect.com

ScienceDirect

ELSEVIER

Identification of a Function-Specific Mutation of Clathrin Heavy Chain (CHC) Required for p53 Transactivation

Hirokazu Ohata[1,2], Nobuyuki Ota[3], Mikako Shirouzu[4], Shigeyuki Yokoyama[4,5], Jun Yokota[2], Yoichi Taya[6]* and Masato Enari[1,2]*

[1]*Radiobiology Division, National Cancer Center Research Institute, Tsukiji 5-1-1, Chuo-ku, Tokyo 104-0045, Japan*

[2]*Biology Division, National Cancer Center Research Institute, Tsukiji 5-1-1, Chuo-ku, Tokyo 104-0045, Japan*

[3]*A-Cube Inc. and Musashino University, Research Institute of Pharmaceutical Sciences, Tokyo, Japan*

[4]*Systems and Structural Biology Center, RIKEN Yokohama Institute, 1-7-22 Suehiro-cho, Tsurumi, Yokohama 230-0045, Japan*

[5]*Department of Biophysics and Biochemistry, Graduate School of Science, The University of Tokyo, 7-3-1 Hongo, Bunkyo-ku, Tokyo 113-0033, Japan*

[6]*Cancer Science Institute of Singapore, National University of Singapore, Center for Life Sciences, #02-07, 28 Medical Drive, Singapore 117456*

Received 19 June 2009; received in revised form 14 September 2009; accepted 14 September 2009
Available online 18 September 2009

Edited by P. Wright

The p53 pathway is activated in response to various cellular stresses to protect cells from malignant transformation. We have previously shown that clathrin heavy chain (CHC), which is a cytosolic protein regulating endocytosis, is present in nuclei and binds to p53 to promote p53-mediated transcription. However, details of the binding interface between p53 and CHC remain unclear. Here, we report on the binding mode between p53 and CHC using mutation analyses and a structural model of the interaction generated by molecular dynamics. Structural modeling analyses predict that an Asn1288 residue in CHC is crucial for binding to p53. In fact, substitution of this Asn to Ala of CHC diminished its ability to interact with p53, leading to reduced activity to transactivate p53. Surprisingly, this mutation had little effect on receptor-mediated endocytosis. Thus, the function-specific mutation of CHC will clarify physiological roles of CHC in the regulation of the p53 pathway.

Keywords: clathrin heavy chain; p53; structural modeling; transcription; tumor suppressor

*Corresponding authors. E-mail addresses: csiyt@nus.edu.sg; menari@ncc.go.jp.

Abbreviations used: ActD, actinomycin D; BSA, bovine serum albumin; CHC, clathrin heavy chain; CLC, clathrin light chain; DMEM, Dulbecco's modified Eagle's medium; GST, glutathione S-transferase; HRP, horseradish peroxidase; MCSA-PCR, multi-conformation simulated annealing pseudo-crystallographic refinement; PARP, poly-ADP ribose polymerase; RT-PCR, reverse transcriptase–polymerase chain reaction; UTR, untranslated region.

Introduction

The tumor suppressor p53 protein is a transcription factor that protects cells from malignant transformation. The p53 pathway is activated in response to various cellular stresses such as DNA damage, oncogene activation, and hypoxia. Upon activation, p53 exerts its tumor suppressor activity by inducing cell-cycle arrest, apoptosis, or senescence.[1–3] Because mutations in the p53 gene have been found in around 50% of human cancers and most mutations of p53 in tumors are located in the central DNA-binding domain, transcriptional regulation by p53 is thought to be most important for prevention of tumorigenesis.[4] Thus, analysis of p53-mediated transcriptional mechanisms is indispensable for elucidation of tumorigenesis and development of new antitumor drugs. Although many factors that contribute to the regulation of p53 activity have been reported,[1,5,6,9] detailed mechanisms remain to be elucidated.

We have previously reported that clathrin heavy chain (CHC), which is a cytosolic protein involved in receptor-mediated endocytosis and intracellular trafficking and recycling of receptors,[10–12] is present in nuclei and enhances p53-mediated transcription.[13] The presence of CHC in nuclei and nuclear matrices was confirmed by other groups.[13–15] We have also shown that p53 interacts with CHC not only in nuclei but also in cytosol and regulates clathrin-mediated endocytosis through the association with CHC.[16]

In the clathrin-mediated endocytic pathway, clathrin is composed of a trimer of CHC and is associated with each clathrin light chain (CLC), called triskelion, and they further assemble to form a polyhedral cage-like structure.[17] Polyhedral clathrin is recruited to the plasma membrane and promotes the internalization and recycling of receptors participating in signal transduction events.[18] CHC consists of an N-terminal β-propeller domain that is necessary for binding to adaptor proteins for the internalization of various molecules, followed by seven α-helical repeat structures named 'clathrin repeats'.[17] In addition, it has been reported that CHC plays a role in mitosis.[19] In the C-terminus, CHC possesses a trimerization domain essential for stable formation of the polyhedral clathrin structure and CLC-binding domain.[20] We have recently reported that CHC bearing residues from 833 to 1406 (CHC833–1406) lacking trimerization and CLC-binding domains interact with p53 and enhance p53 transactivation.[21] Thus, the oligomerization of CHC, which is critical for endocytosis and mitosis,[20,22,23] has not been necessary for p53-mediated transcription, supporting our proposition that CHC has an alternative function as a co-activator for p53 and an additional role in the regulation of endocytosis and mitosis.[21] However, although our findings support that CHC functions as a co-activator of p53, there is a limitation to investigate the physiological roles of CHC in the p53-mediated pathway because CHC ablation in examining the impact on p53 transactivation may cause some effects on vesicle transport and endocytosis. Therefore, the exploration of function-specific mutations of CHC for the p53 pathway is important for elucidation of mechanisms by which CHC transactivates p53.

We have previously found that there is a considerable similarity between p53 and CLC in the CHC-binding region.[13] However, the detailed binding interface between p53 and CHC remains to be determined. Thus, the construction of a structural model of the p53–CHC interface provides further insights into regulation of p53 transactivation by CHC. In this study, we show that conserved hydrophobic residues between p53 and CLC are important for p53 transactivation and that p53 function correlates positively with the interaction with CHC. Moreover, *in silico* structural prediction of the interface between p53 and CHC reveals that the Asn1288 residue in CHC is essential for binding to p53. Interestingly, the substitution of this Asn to Ala (CHC-N1288A) diminishes its ability to transactivate p53 without any effect on receptor-mediated endocytic activity.

Results

Conserved residues between p53 and CLC are required for the interaction with CHC to enhance p53 transactivation

We have previously reported that the N-terminal region of p53 is required for binding to CHC using various deletion mutants of p53.[13,21] In our previous report, we noticed a significant similarity of the N-terminal transactivation domain of p53 to the CHC-binding region of CLC and that various hydrophobic residues are conserved in human p53 (Fig. 1a).[13] To assess whether these conserved residues are required for the interaction with CHC, we generated four p53 point mutants (L43A, I50A, L43A/I50A, and W53R) as glutathione *S*-transferase (GST) fusion proteins and carried out an *in vitro* binding assay using ^{35}S-labeled CHC as described previously.[15] A GST pull-down assay showed that the CHC-binding affinity of all p53 proteins bearing mutations in conserved residues is lower than that of wild-type p53 (Fig. 1b). Furthermore, we assessed the effect of p53 mutations on the binding to endogenous CHC in cells. FLAG-tagged p53 proteins were expressed in p53-null cells, and cell lysates were immunoprecipitated with anti-FLAG antibody followed by immunoblotting with indicated antibodies. Immunoprecipitation assay shows that these mutations cause reduced interaction with CHC (Fig. 1c).

To examine the effect of these p53 mutants on p53 transactivation, we performed reporter assays using promoters of p53-target genes. Reporter assays using various p53 mutants show that mutations of p53 at N-terminal conserved residues cause marked reduction of transactivation of p53-target genes such as p53AIP1 (Fig. 2a) and p21 (Fig. 2b). To confirm

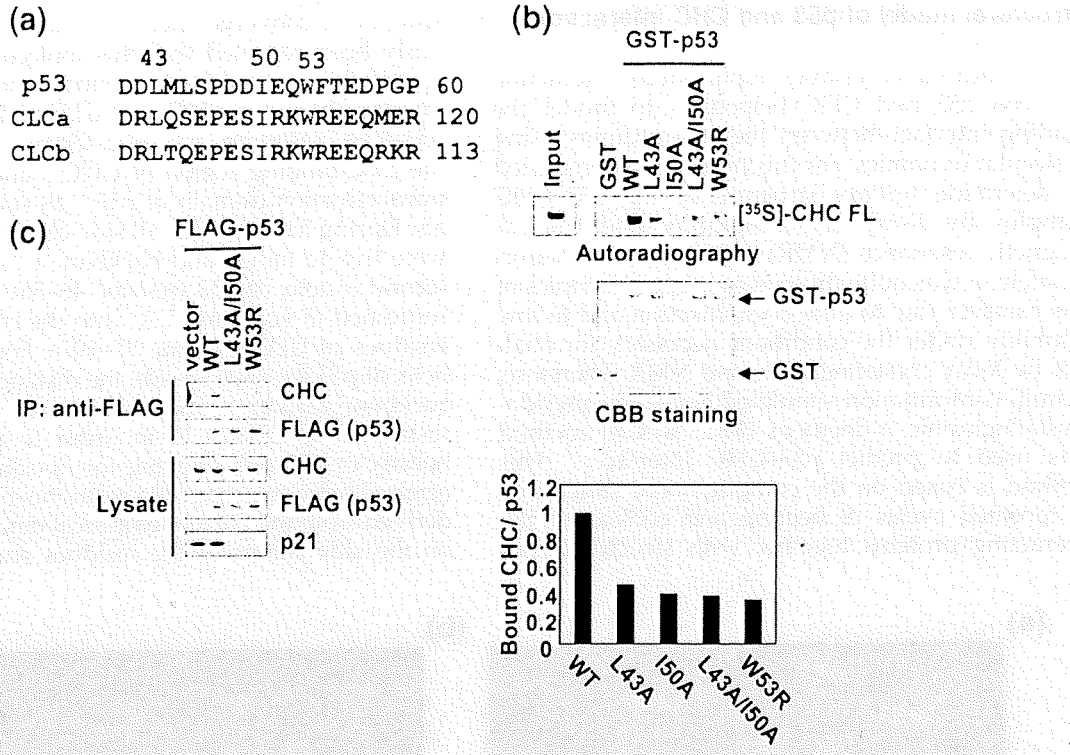

Fig. 1. Conserved residues in p53 are required for the interaction with CHC. (a) Alignments of the CHC-binding region of human p53, CLCa, and CLCb. (b and c) Conserved residues in p53 are required for interaction with CHC. (b) ^{35}S-labeled full-length CHC was synthesized by an *in vitro* transcription-coupled translation system using rabbit reticulocyte lysates. Lysates containing ^{35}S-labeled CHC were mixed with GST or GST-p53 derivatives immobilized on glutathione-Sepharose 4B beads for binding assay (upper panel). GST and GST-p53 proteins used for binding assay were stained by CBB (middle panel). The graph represents the ratio of bound CHC to GST or GST-p53, as quantified by Image J densitometry (lower panel). (c) H1299 cells were transfected with each FLAG-p53 construct. FLAG-p53 proteins in cell lysates were immunoprecipitated by anti-FLAG M2 agarose, and eluates were separated by SDS-PAGE, followed by immunoblotting with indicated antibodies.

the effect of substitutions of these conserved residues on p53 transactivation, we examined the induction of endogenous p53-target genes by immunoblotting. Although the expression level of mutated p53 proteins was the same as that of wild-type p53, the induction of p53-responsive genes such as p21 and Mdm2 by ectopic expression of mutated p53 proteins was strikingly reduced compared with that of wild-type p53 (Fig. 2c). These results suggest that the ability of p53 to bind to CHC correlates with p53 transactivation and indicates that conserved hydrophobic residues between p53 and CLC are important for the transcriptional activity of p53 as well as binding to CHC.

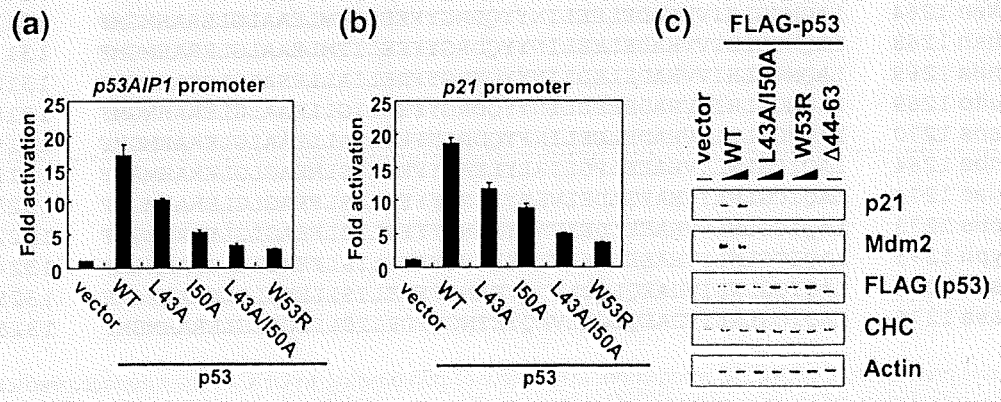

Fig. 2. p53 transactivation correlates with the ability of p53 to bind CHC. (a and b) Conserved residues in p53 are required for p53 transactivation. H1299 cells were transfected with each p53 construct and the p53AIP1 reporter plasmid (a) or p21 reporter plasmid (b), and luciferase activity was measured 24 h after transfection. (c) H1299 cells were transfected with each p53 construct, and whole-cell lysates were analyzed by immunoblotting using the indicated antibodies. Actin was used as a loading control.

Structural model of p53 and CHC interaction

Identification of residues important for interaction between p53 and CHC helped us to model the binding interface between the two proteins using molecular dynamics. For this purpose, we first tried to determine tertiary structure of the p53–CHC complex by X-ray crystallography and nuclear magnetic resonance (NMR) techniques, but unfortunately, it was quite difficult to prepare samples of this complex due to little crystallization and to low solubility under the conditions necessary for analysis by X-ray crystallography and NMR. Therefore, a multi-conformation simulated annealing pseudo-crystallographic refinement (MCSA-PCR) method was used to predict p53–CHC interface.[34] This method is based on the computational simulation of repeated cycles of heating and cooling of the interacting proteins together with structural constraints to converge their structures. It has previously been reported that this molecular dynamics approach was used for preliminary modeling of the interface between CHC and CLC.[35] To model the p53–CHC interface, we used tertiary structures of the CLC-binding region of CHC[35] and N-terminal transactivation domain of p53[20] as starting materials. During MCSA-PCR, all side-chain atoms of p53 were free to move, and backbone C$^{\alpha}$ atoms in the second α-helix of p53 (residue 46–56) were weakly restrained (5 kcal mol^{-1} Å^{-2}) to the corresponding residues of CLC (residue 97–107). For the first α-helix of p53 (residue 35–40), the distances of the p53 backbone carbonyls and amides were also weakly restrained to 2.86±1 Å in order to promote the helicity of p53 but allowing for deviation from the original helix structure. No restraints or constraints derived from the current empirical data are applied on the side chains of the residues studied in this

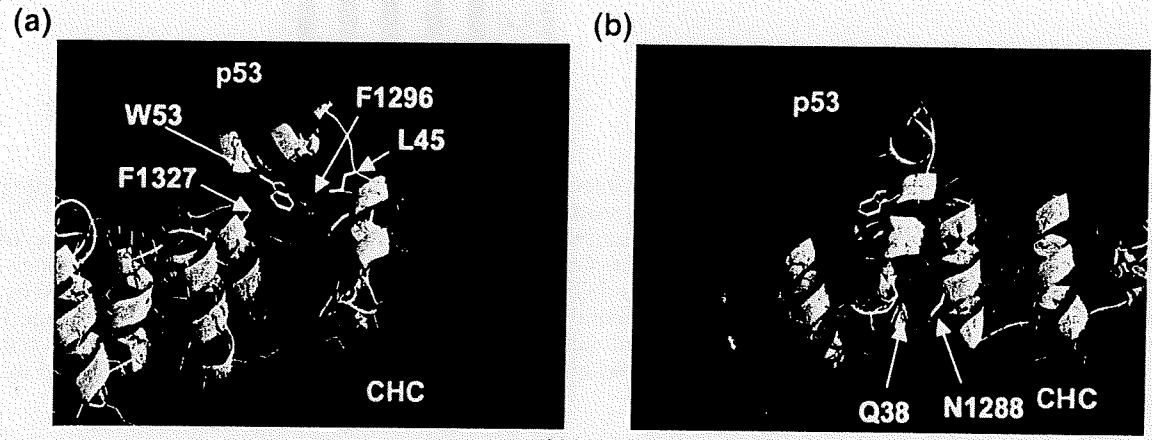

(c)

N1288 ↓

Human 1268	LAQMCGLHIVVHADELEELINYYQDRGYFEELITMLEAALGLERAHMGMF	1317
Chimpanzee 1268	LAQMCGLHIVVHADELEELINYYQDRGYFEELITMLEAALGLERAHMGMF	1317
Dog 1281	LAQMCGLHIVVHADELEELINYYQDRGYFEELITMLEAALGLERAHMGMF	1330
Cattle 1268	LAQMCGLHIVVHADELEELINYYQDRGYFEELITMLEAALGLERAHMGMF	1317
Mouse 1268	LAQMCGLHIVVHADELEELINYYQDRGYFEELITMLEAALGLERAHMGMF	1317
Rat 1268	LAQMCGLHIVVHADELEELINYYQDRGYFEELITMLEAALGLERAHMGMF	1317
Chicken 1264	LAQMCGLHIVVHADELEELINYYQDRGYFEELITMLEAALGLERAHMGMF	1313
Zebra fish 1268	LAQMCGLHIVVHADELEELINYYQDRGYFEELITMLEAALGLERAHMGMF	1317
Drosophila 1269	LAQMCGLHIVVHADELEDLINYYQNRGYFDELIALLESALGLERAHMGMF	1318
Mosquito 1269	LAQMCGLHIVVHADELEDLINYYQDRGYFEELIGLLEAALGLERAHMGMF	1318
C. elegans 1270	LAQMCGLHIVVHADELEELINFYQDRGHFEELIALLEAALGLERAHMGMF	1319
S. pombe 1264	LAQICGLNLIVHAEELPGLIRLYEERGYFEEVISLMEAGLGLERAHMAFY	1313
S. cerevisiae 1274	LAQICGLNLIVHAEELDELVERYESNGYFEELISLFEAGLGLERAHMGMF	1323
K. lactis 1273	LAQICGLNLVVHAEELDELVAVYEHNGYFEELISLFEAGLGLERAHMGMF	1322
E. gossypii 1275	LAQICGLNLIVHAEELKELVDKYESNGYFEELISLFEAGLGLERAHMGMF	1324
M. grisea 1276	LAQICGLNLIVDAEQLQTLVKQYERNGFFDELISLLENGLGLERAHMGMF	1325
N. crassa 1276	LAQICGLNLIVDAEQLQALVKQYETNGYFDELISLLEQGLGLERAHMGMF	1325

Fig. 3. Structural prediction of p53–CHC interaction. (a) A view of p53 binding to CHC at the interface predicted by molecular dynamic simulation. p53 is in cyan and CHC is in green. The aromatic side chain of Trp53 of p53 mediates the interaction with an aromatic side chain of Phe1327 in the hydrophobic cleft of CHC. The side chain of Leu45 of p53 interacts with the aromatic side chain of Phe1296 of CHC through hydrophobic interaction. (b) Structural modeling revealed that the side chain of Asn1288 of CHC is close to the side chain of Gln38 of p53. (c) Asn1288 in CHC is conserved in multicellular organisms from mammals to flies, but this amino acid residue is not present in unicellular organisms such as yeasts and fungi.